KONINKLIJK NEDERLANDS METEOROLOGISCH INSTITUUT

WETENSCHAPPELIJK RAPPORT

SCIENTIFIC REPORT

W.R. 82 - 6

H. van Dop, B.J. de Haan and C. Engeldal

The KNMI mesoscale air pollution model

De Bilt, 1982

Publikatienummer: K.N.M.I. W.R. 82-6 (FM)

Koninklijk Nederlands Meteorologisch Instituut =
Royal Netherlands Meteorological Institute,
Fysisch Meteorologisch Onderzoek = Physical
Meteorological Research,

P.O. Box 201,

3730 AE De Bilt,

The Netherlands.

U.D.C.: 551.510.42

CONTENTS

Samenvatting

In 1978 werd op het KNMI, deels gefinancierd door het Ministerie van Volksgezondheid en Miliehygiëne, een project gestart dat "de formulering van het transport van luchtverontreiniging over lange afstand" tot doel had. Het te ontwikkelen model moest "ten behoeve van de beleidsvoorbereiding inzake de luchtverontreiniging informatie verschaffen over de relatie tussen emissies en de te verwachten concentraties op afstanden tot 500 km, zowel voor grote oppervlakte bronnen als voor hoge schoorstenen". In deze samenvatting zal een korte beschrijving worden gegeven van het ontwikkelde model, en zullen de belangrijkste uitkomsten worden samengevat.

Het model is ontwikkeld met als primaire toepassing Nederland en omgeving, doch het is in principe geschikt voor ieder ander willekeurig vergelijkbaar vlak gebied van dezelfde afmeting (ca. 500 x 500 km^2). De atmosferische laag die door het model beschreven wordt strekt zich uit tot een hoogte van 600 m. De ervaring leert dat luchtverontreiniging zich voornamelijk tot deze laag beperkt. Verder kan gesteld worden dat vrijwel alle bonnen zich in deze laag bevinden. Het model voorziet in de berekening van uurlijkse concentratie-waarden over perioden van enige dagen. In dit tijdsbestek variëren de voor de verspreiding van luchtverontreiniging relevante meteorologische omstandigheden aanzienlijk. Bij de beschrijving van met name de verticale verspreiding is hiermee als volgt rekening gehouden.

1. Horizontale en verticale verspreiding.

- 's Nachts ontwikkelt zich meestal een stralingsinversie die zich als regel uitstrekt tot een hoogte van een paar honderd meter. In deze laag wordt de verspreiding van luchtverontreiniging bepaald door het met de hoogte sterk varierende horizontale windveld, en de (zwakke) turbulentie die hoofd-zakelijk de verticale verspreiding veroorzaakt. Boven deze laag wordt de turbulentie zo gering geacht dat alleen het horizontale windveld tot de verspreiding bijdraagt.
  De inversiehoogte en het windveld worden indirect uit de synoptische waarnemingen bepaald.

- In de loop van de ochtend verandert de atmosferische stabiliteit, met als gevolg dat de turbulentie en dus ook de verticale verspreiding zal toenemen. Dit heeft enerzijds tot gevolg dat verontreiniging dicht bij het aardoppervlak zich naar grotere hoogten kan verplaatsen, doch anderzijds

dat verontreiniging in hogere luchtlagen het aardoppervlak kan bereiken (fumigatie). De aan het aardoppervlak grenzende turbulente laag wordt de menglaag genoemd. In de loop van de dag kan de bovenste begrenzing van deze laag een hoogte bereiken van 1 à 2 km. Dit proces en de mate van verdunning van luchtverontreiniging die hiervan het gevolg is worden door het model beschreven.

- Gewoonlijk zal zich in de namiddag opnieuw een stralingsinversie ontwikkelen waarmee de hier beschreven kringloop gesloten wordt. Het 3-dimensionale windveld dat noodzakelijk is voor de beschrijving van het horizontale transport, is afgeleid uit de synoptische waarnemingen binnen het gebied. het is gebaseerd op uurlijkse rapporten van de wind op 10 m hoogte, alsmede op, van de drukwaarnemingen afgeleide, drukgradienten. Ook de windgegevens op enige hoogte - verkregen uit ballonoplatingen en (televisie) toren of mastwaarnemingen - zijn gebruikt.
  Een schatting van de verticale verspreiding is mede gebaseerd op de uitkomsten van een met dit project parallel lopend onderzoek getiteld: "Klimatologie van de stabiliteit", dat eveneens gedeeltelijk door het Ministerie werd gefinancierd.

2. Depositie en Chemische processen.

Vrijwel alle verontreiniging komt na enige tijd weer op het aardoppervlak terecht. Voor een groot aantal luchtverontreinigingscomponenten geldt dat een aanzienlijk percentage al binnen enkele dagen weer uit de atmosfeer is verdwenen. We onderscheiden natte en droge depositie. In beide gevallen kunnen ook chemische processen in de atmosfeer een meer of minder belangrijke rol spelen.

- Droge depositie.
  Deze wordt door het model beschreven door middel van het "depositiesnelheid" concept, waarbij het verlies door depositie evenredig wordt verondersteld aan de concentratie nabij het aardoppervlak. De empirische evenredigheidsconstante hangt af van de combinatie van chemische eigenschappen van verontreinigingscomponent en bodemtype. Voor o.a. dit doel is een gedetailleerde beschrijving van het gebied (topografie) gemaakt.
- Natte depositie.
  Hieronder verstaan we de verontreiniging die via de neerslag weer op het aardoppervlak terecht komt. De keten van fysische en chemische processen met

dit eindresultaat is uitermate gecompliceerd en slechts ten dele begrepen. Om toch het effect van dit proces op de luchtconcentraties enigszins in rekening te kunnen brengen is in het model verondersteld dat bij optredende neerslag een afname van luchtverontreiniging plaatsvindt, die evenredig is met de heersende concentratie. Ook in dit geval is de evenredigheids-constante gebaseerd op waarnemingen en experimenten.

- Atmosferische chemie.
  Hiervoor geldt in zekere mate ook wat voor natte depositie geldt. In het model wordt de atmosferische chemie eveneens met een op waarnemingen gebaseerde vervalconstante beschreven. Dit maakt het model in zijn huidige vorm ongeschikt voor de beschrijving van de verspreiding van die luchtver-ontreinigingscomponenten waarbij (foto)chemische processen een belangrijke rol spelen.

3. Resultaten.

Na een uitvoerige test van een aantal (numeriek) wiskundige aspecten is het model getest in een proefperiode (29 en 30 mei 1978), waarbij gebruik gemaakt werd van een realistisch SO_2-emissiebestand. De resultaten van deze analyse laten zich als volgt samenvatten.

- De meteorologische condities weerspiegelen zich in de concentratieverdeling, d.w.z. overdag een homogeen vertiale concentratieverdeling, terwijl 's nachts de concentraties sterk met de hoogte variëren.
- De invloed van de mate van droge depositie op het concentratiepatroon is aanzienlijk.
- Het fumigatieproces - dat regelmatig de grondconcentraties beïnvloed gedurende de ochtenduren - wordt goed door het model beschreven.
- De benodigde rekentijd voor de simulatie van een etmaal bedraagt ca. 30 minuten op een middelgrote computer (Burroughs 6800), waardoor het model zich uitstekend leent voor praktische toepassingen. Hierbij dient te worden opgemerkt dat de inzameling, analyse en bewerking van de meteorologische invoergegevens een tijdrovende procedure is.

4. Toepassingen en perspectieven.

De modeluitkomsten zijn niet vergeleken met gemeten concentratiewaarden in het gebied: Onzekerheid in de opgegeven emissies en emissiehoogten, onbekendheid met de hoeveelheid luchtverontreiniging die het modelgebied binnenstroomt en de initiële concentratieverdeling, alsmede de onnauwkeurigheden in de metingen

maken dat een dergelijke vergelijking mogelijk meer vragen zou oproepen dan beantwoorden. Niettemin is de beantwoording van de vraag naar de kwaliteit van het beschreven model gewenst. In dit kader, is deels in internationaal verband, een vervolgstudie ondernomen die, beoogt de "prestaties" en mogelijkheden van een vijftal modellen, waaronder het hier beschrevene, te onderzoeken. Op basis van de resultaten van deze studie zal een uitspraak gedaan kunnen worden over de gebruikswijze en -waarde van deze modellen als beleidsinstrumenten.
Het model zal worden toegepast in het kader van het rekensysteem luchtverontreiniging, bij het bepalen van de invloed op de luchtkwaliteit van beleidsmaatregelen van het ministerie van Volksgezondheid en Milieuhygiene.

Het model is geschikt voor het uitvoeren van diverse studies, bijv.:

1) Scenario-studies bij industriële planning,
2) Quantificering van grensoverschrijdende luchtverontreiniging,
3) Differentiatie van concentraties op leefniveau naar bronherkomst (bijv. hoge vs. lage bronnen, verkeer vs. industrie).
4) Het maken van gevoeligheidsanalyses en modelvergelijkingsstudies waarbij het als referentie model kan dienen voor andere luchtverontreinigingsmodellen, waarin de meteorologie minder gedetailleerd is opgenomen.
5) Het model zou een basiselement kunnen zijn voor een fotochemisch model. De gevolgde numerieke methodiek en de modulaire opbouw maken de invoering van complexe atmosferische chemie tamelijk eenvoudig.
6) In de nabije toekomst kan verwacht worden dat over steeds meer gedetailleerde prognostische meteorologische verschijnselen beschikt kan worden. In dat geval zou het model ook in prognostische zin gebruikt kunnen worden en bijv. kunnen worden ingezet bij calamiteiten (accidentele lozingen) en verwachtingen tijdens z.g. luchtverontreinigingsepisodes.

Abstract

An air pollution model is developed which describes the transport of pollutants on a scale of 500 x 500 km^2. This corresponds with episodes of a few days. In the model a detailed description is given of the vertical diffusion processes under different stability conditions. Also much effort is put into the determination of the horizontal mean wind field, which is strongly non-homogeneous and non-stationnary on the above space- and timescales. The transport equation is solved numerically. For the advective part a pseudo-spectral scheme is applied. The vertical diffusion is treated with a Crank-Nicolson scheme. Dry deposition is included in the model in a way which accounts for the chemical properties of pollutant and soil. Wet deposition and chemical transport are included by simple linear decay terms. The model is tested in a complex source area (Netherlands and surrounding countries), during a fair weather episode on 29 and 30 May 1978. The model gives a satisfactory description of the fumigation process. Also other diurnal variations in atmospheric stability are well reflected in the concentration distribution. The effect of dry deposition is studied. The moderate computer time requirements make the model particularly apt for practical applications.

1. Introduction.

The production of waste material is inherent to any kind of activity in our society. In the past this was not really considered a problem because the intensity and density of waste production was not large enough compared with the absorbing capacity of the environment.
The industrial revolution and the exponential growth of world's population changed this relation drastically. Nowadays each highly populated region, where the energy consumption per caput - a fair measure for human and economic activity - is high, is confronted with a waste problem. Moreover, the public acceptance of a certain degree of air pollution has decreased.
Besides the trivial solution, which is the reduction or evasion of any process which produces waste materials in undesired quantities, there exist in general two approaches to circumvent adverse effects of pollution.

- The first consists of concentrating the waste material in small volumes, and storage in places which are thought to have a negligible interaction with the ecosystem (storage in the soil, at the seabottom, or at deserted sites).
- The second method is quite the opposite of the first and consists of the dilution of waste material to such an extent that it is considered harmless to the environment (dumping in rivers, lakes etc., and the atmosphere).

Both an advantage and disadvantage of the latter method is that nature itself takes care of the dilution: it is a cheap (economic) way of disposal, but we loose largely the control over the fate of these pollutants, and consequently, over their possible impact on the environment. Here we enter the terrain of the environmental policy and decision makers, who want answers with respect to the whereabouts of matter released in water or air.
We will restrict ourselves in the following to air pollution, where the major questions are:

- what is the spatial and temporal distribution of the released material, and
- where, and in which form and quantity is the released material deposited on the earth surface?

Air quality models play an important role in these questions. Together with observations they give an insight - though still far from perfect - in the

complex physical and chemical processes, which are involved in the dispersion, transformation and deposition of pollutants. Yet they are indispensable now in

- decisions on industrial site planning,
- the determination of the relative contribution of the different source categories to the ambient concentration (e.g., traffic versus industrial sources, foreign versus national sources),
- the development of air pollution control strategies.

The residence time of material in the atmosphere may vary from a few hours to many years, so that the spatial scale which should be covered varies from a few km's to the global scale. The non stationarity and non homogeneity of the (turbulent) transport processes complicates the description on this wide range of scales considerably. Therefore, air quality models cover only a limited range in space and time.

It would take us too far to discuss all the aspects of modelling on the various scales. We may refer to a review of air quality models given by Van den Hout and Van Dop (1981) and Young (1981).

In the present report a mesoscale air quality model is considered which describes the transport of pollution on a scale of ~ 500 km, which corresponds with a time scale of one or two days. On this scale we encounter a broad variety of atmospheric conditions. Also, wet and dry deposition and atmospheric chemistry play an important role. Therefore, this type of model is rather complicated and, as a consequence, the majority is still in a research version.

Another problem which is encountered is that the verification of these models is difficult, because of the lack of accurate emission data of many air pollution components.

The model which we describe here emphasizes the description of the transport process, though the other processes involved will not be neglected.

In the next section we shall give an outline of the model. In section 3 we will present some results. The appendices provide more detailed information on the various model aspects.

2. Model Outline

2.1. Introduction

The model should provide hourly concentrations with sufficient spatial resolution, in an area of ~ 500 x 500 km^2 and up to a height of ~ 500 m, during episodes of a few days. The description of transport and diffusion has been guided by our present knowledge of the (idealized) diurnal variation of meteorological conditions of the atmospheric boundary layer.
The three essential assumptions are:

i. During nighttime within a relatively short time, a stable layer develops, which extends up to a boundary-layer height, z_i. In the model an average (but time dependant) over land value is used. In this layer air pollution is assumed to be transported by the (hourly) mean horizontal flow and by vertical diffusion only. At heights larger than z_i, the vertical diffusion will be neglected, so that pollutants are only horizontally displaced by the mean wind.

ii. When during the morning hours the atmospheric stability changes due to surface heating by the enhanced irradiation, the nocturnal inversion erodes and an unstable mixed layer develops. In the initial stage of the mixed-layer development vertical diffusion is still moderate. However, when the mixed-layer exceeds a fixed height*), it is assumed that turbulence mixes the pollutants throughout the layer in such short times that vertical concentration gradients will be considered negligible. During the inversion rise the concentrations may change due to the entrainment of pollutants present in the adjacent upper layer (fumigation).

iii. In the late afternoon a new ground-based stable layer develops. The pollution which - at that time - is present above 600 m will usually be advected outside the considered area during the night to come, so that it will not influence concentrations during the next day, when a new mixed-layer develops. Sources outside the area are not taken into account.

Besides transport also dry and wet deposition and (linear) chemistry is considered. A summary of the above sketched assumptions is depicted in Fig. 1.

*) at present 600 m. We assume that all sources emit below this value.

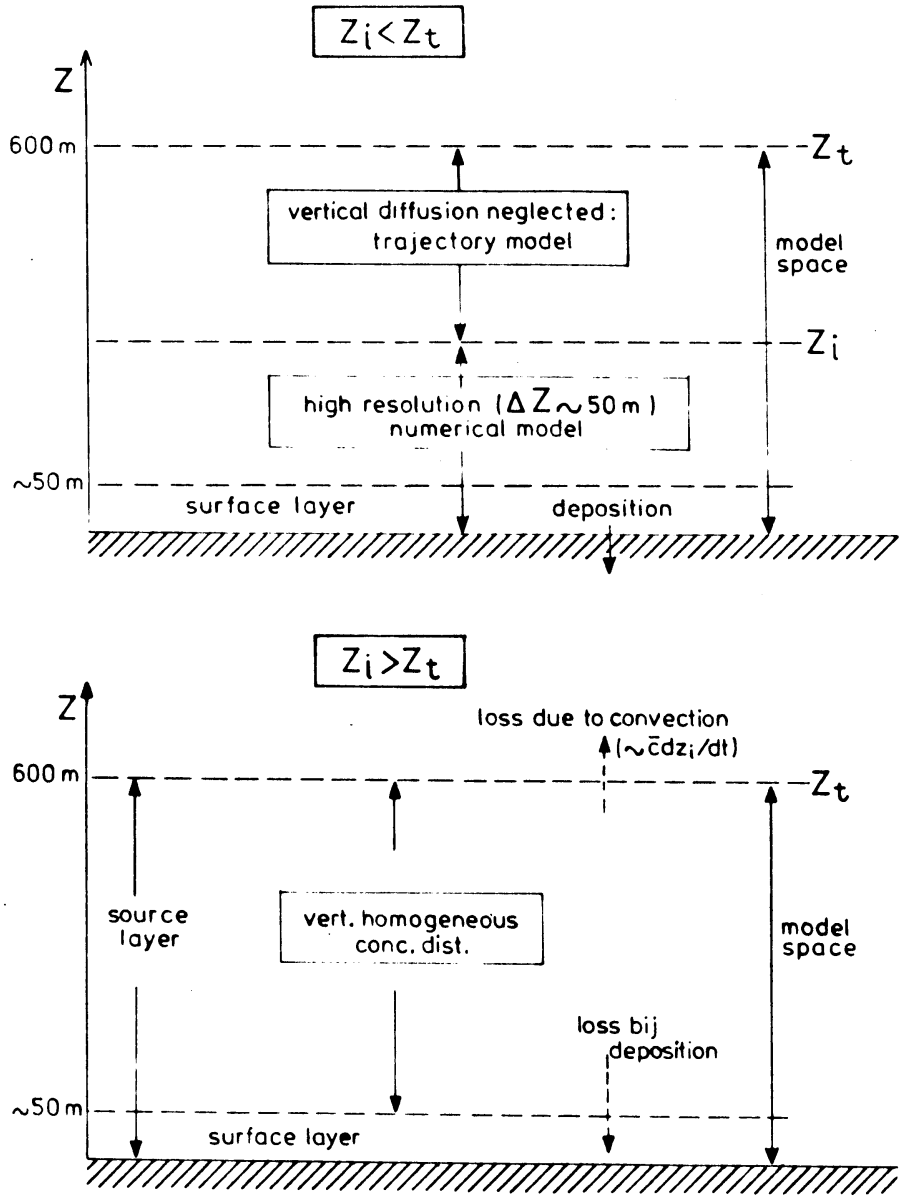

Fig. 1. Graphical presentation of the model concept. Along the vertical axis the height above the surface is indicated. The inversion height is denoted by z_i. The grid model extends to z_t (= 600 m). Two cases are distinguished: (a) the inversion depth (or mixed layer height) z_i does not exceed z_t, and (b) the inversion height exceeds z_t (daytime conditions).

2.2. Mathematical Framework

2.2.1. The transport equation.

The transport equation is derived from the continuity equation,

$$\partial C/\partial t + U\ \partial C/\partial x + V\ \partial C/\partial y = \partial/\partial z\ (K_z\ \partial C/\partial z) + S\ . \qquad (2.1)$$

Here $C(x,y,z,t)$ denotes the hourly average concentration and U, $V(x,y,z,t)$ the horizontal components of the wind field*. The vertical turbulent transport ($\overline{cw}$) is through first order closure (Pasquill, 1974) expressed as

$$\overline{cw} = -\ K_z\ \partial C/\partial z\ , \qquad (2.2)$$

where $K_z(x,y,z,t)$ is the eddy diffusivity. The term $S(x,y,z,t)$ contains all the sources and sinks, which will be discussed below.
In (2.1) the horizontal turbulent diffusion terms $\overline{cu}$ and $\overline{cv}$ are omitted. This assumption can be justified by the following argument.
Equation (2.1) can in its general form only be solved numerically, i.e. by rewriting (2.1) into finite difference form. The considerations which lead to a particular choice of the horizontal gridsize can be of various nature.In general the size will be of the same order of(or larger than) the spatial resolution of the meteorological and air pollution observation network. Once the gridsize is fixed, say Δ, one may neglect horizontal diffusion when its scale is smaller than the gridsize, or

$$\sigma \lesssim \Delta\ , \qquad (2.3)$$

where σ is a measure for the horizontal diffusion. For Fickian (constant K) diffusion, σ is related to an eddy diffusivity K by:

$$\sigma = (2Kt)^{\frac{1}{2}}\ , \qquad (2.4)$$

where t is the travel time. It is reasonable to assume that $K \sim q\Delta$, since motions on a scale larger than Δ are resolved by, and contained in the gridvalues of U and V. The order of magnitude of the turbulent velocity is given by q.
An upper limit for σ can be found by putting $t = D/U$, where D is the linear dimension of the considered region. We can write the condition (2.3) then as

* Capital symbols denote average values. The fluctuating components are indicated by lower case symbols.

$$\Delta \gtrsim 2\ D\ q/U\ . \qquad (2.5)$$

D can be written as $n\Delta$, where n is the number of gridpoints in a horizontal direction. Taking $q \sim 0.3\ ms^{-1}$ and $U \sim 6\ ms^{-1}$, (2.5) implies that when $n \lesssim U/2q = 10$ it is not required to include horizontal diffusion. Though in our case n=16, we assume that the number of grid points is small enough to be consistent with the negligence of horizontal diffusion.

In (2.1) also the mean vertical velocity is neglected. This is generally justified over more or less flat terrain. Indeed, the topography of the model region (Fig. 2), does not reveal very significant differences in terrain height.

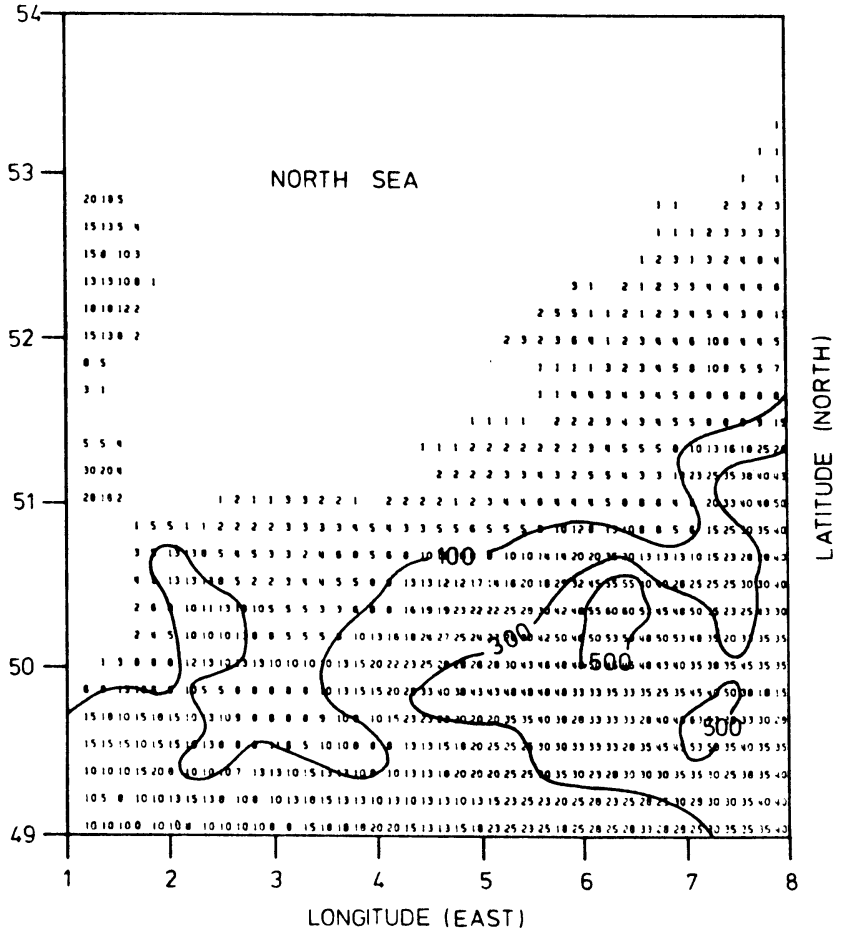

Fig. 2. Average height of the region (numbers are in decameters). Each number corresponds with an area of 10'x10' arc minutes. The region extends from 49°-54° N and 1°-8° E. Isopleths of 100, 300 and 500 m are indicated by the solid lines.

When vertical diffusion is considered negligible (2.1) reduces to the advection equation:

$$\partial C/\partial t + U\ \partial C/\partial x + V\ \partial C/\partial y = S\ . \qquad (2.6)$$

Equation (2.6) is used above the inversion and mixed layer.

Also in strong turbulent (well-mixed) conditions (2.1) can be simplified: we introduce a mixed-layer average concentration,

$$\overline{C} = \frac{1}{h(t)} \int_o^{h(t)} C(z)dz\ . \qquad (2.7)$$

Integration of (2.1) with respect to z and multiplication with 1/h yields:

$$\frac{1}{h} \int_o^h \frac{\partial C}{\partial t}\, dz + U\ \partial\overline{C}/\partial x + V\ \partial\overline{C}/\partial y = \overline{S} + K_z\ \partial C/\partial z \Big|_o^h\ , \qquad (2.8)$$

where we have assumed that U and V are independent of z in well-mixed circumstances, e.g., in the x-direction we make the approximation

$$\frac{1}{h} \int_o^h U \frac{\partial C}{\partial x}\, dz \simeq U \frac{\partial \overline{C}}{\partial x}\ . \qquad (2.9)$$

The term $K_z \partial C/\partial z$ is the vertical turbulent flux which is taken equal to zero at the top. At $z = 0$ it describes the flux to the surface or dry deposition, which will be discussed below. Meanwhile the term is absorbed in $\overline{S}$. Integrating the first term by parts, using:

$$\frac{\partial}{\partial t} \int_o^h C\ dz = \frac{dh}{dt} C(h) + \int_o^h \frac{\partial C}{\partial t}\, dz\ ,$$

and putting $C(h) = 0$, which is equivalent with assuming that unpolluted air is entrained, the result is:

$$\partial\overline{C}/\partial t + U\ \partial\overline{C}/\partial x + V\ \partial\overline{C}/\partial y = -\ (\overline{C}/h)dh/dt + \overline{S}\ . \qquad (2.10)$$

Equations (2.1, 2.6 and 2.10) constitute the three main model equations.

2.2.2. Initial and boundary conditions.

Initially the region is assumed to be free of contaminants. At $t = 0$ the

sources are "switched on". The concentration build-up will take - dependent on the meteorological conditions - a few hours.
Inflow of material from outside the region is neglected. We assume at the inflow boundary that C = 0 .

It is also assumed that there is no flux of material through the upper boundary. The pollutant flux through the lower boundary is determined by the rate of uptake by the soil. Thus:

$$\begin{aligned} &\text{upper boundary} && : K_z\, \partial C/\partial z = 0 \\ &\text{lower boundary} && : K_z\, \partial C/\partial z = V\, C, \end{aligned} \qquad (2.11)$$

where V(z) is the deposition velocity.
The lowest grid cell extends up to 50 m, which is so close to the surface that it will be most of the time well within the (constant flux) surface layer, so that the deposition velocity V(z) can be expressed in the "standard" deposition velocity at 1 m, V_g, by means of a resistance law,

$$V(z) = \left[r(z,1) + V_g^{-1}\right]^{-1} . \qquad (2.12)$$

The resistance of the layer 1-z is expressed by r(z,1). The deposition velocity V_g is taken from literature (Sehmel, 1980). It depends both on the chemical properties of the surface and the pollutant. The chemical properties of the surface are more or less determined by its overgrowth. For that purpose a classification was made of the various terrain types encountered in the region (appendix A).
The resistance of the layer 1 - z, r(z,1), is given by:

$$r(z,1) = \frac{0.74}{k\, u_*} \left\{\ln(z) - \psi_2(z/L) + \psi_2(1/L\right\} . \qquad (2.13)$$

The stability function ψ_2 is given by:

$$\begin{aligned} &L < 0 : \psi_2 = 2\, \ln\left(\frac{1+y}{2}\right) , \quad y = \left(1 - 9\, \frac{z}{L}\right)^{\frac{1}{2}} \\ &L > 0 : \psi_2 = -6.4\, z/L . \end{aligned} \qquad (2.13a)$$

For the explanation of the other symbols we refer to appendix C,section 3.1. In (2.13a) we have assumed that the transfer of matter and heat is analogous. More details on the deposition can be found in appendix A.

2.2.3. Sources and sinks.

Apart from dry deposition all sources and sinks are contained in the term S (cf. Equation (2.1)).

In fact S stands for

$$S = S(x, y, z, t) + S_w + S_c \,, \tag{2.14}$$

where S(x,y,z,t) is the source function, which contains all surface- and point sources in the area.

Surface sources are introduced at the centres of the lowest grid cells (25 m height). Point sources are introduced at effective stack height, being the physical stack height plus plume rise.

Plume rise is calculated according to Briggs (1969):

$$\begin{aligned} \Delta h &= 109\ Q_H^{3/4}/U \,, \qquad Q_H < 6 \text{ MW}, \\ \Delta h &= 143\ Q_H^{3/5}/U, \qquad Q_H > 6 \text{ MW}. \end{aligned} \tag{2.15}$$

The heat output of the chimney is Q_H. The plume rise (in m) is denoted by Δh, and the average wind speed at stackheight is equal to U. The latter parameter is calculated from the simple power law relation $U = U_{10}\ (z/10)^p$, where for p the value 0.16 (neutral conditions) is used. For simplicity the 10 m wind speed is taken constant and is given a value which is typical for the considered episode.

To avoid too sharp gradients, which result in numerical inaccuracies, it is required to spread out horizontally each source over a few neighbouring grid points.

The removal of pollutants by wet deposition is caused by a complicated chain of processes. It involves cloud dynamics and physical and chemical processes which describe the interaction of liquid water and water vapour in relation with the considered pollutant. An attempt to describe these processes in a simplified way has been made by Fisher (1982). This reseach field is still

developing. Awaiting further results we assume that wet deposition and also chemical removal can simply be described by linear decay:

$$S_w = -k_w C \text{ and } S_c = -k_c C ,$$

where k_w and k_c are decay constants. The wet deposition constant is chosen proportional to the rate of precipitation (Van Aalst en Bergsma, 1981),

$$k_w = \alpha P ,$$

where P is the precipitation rate, and α a constant.
The constant k_c which quantifies the decay by chemical processes, is assumed to be equal to 10^{-2} hr^{-1}.

2.3. Numerical Methods

Equation (2.1) has only analytical solutions for a very limited choice of wind field and eddy diffusivity (Pasquill, 1974, Nieuwstadt and De Haan, 1981a). For arbitrary time and space dependent wind field and diffusivity (2.1) can only be solved numerically. Here, we follow the method of fractional steps, where the solution is obtained by splitting the equation in an advection and a diffusion part:

$$\partial C/\partial t + U\, \partial C/\partial x + V\, \partial C/\partial y = 0 \qquad (2.16a)$$

$$\partial C/\partial t = \partial/\partial z\, (K_z\, \partial C/\partial z) + S . \qquad (2.16b)$$

Equations (2.16a) and (2.16b) are alternatively solved in successive time steps. The advection equation (2.16b) is solved by the so-called "pseudo spectral method" (Gottlieb and Orszag, 1977), an efficient scheme with small numerical errors (see also appendix B and De Haan (1980)). The resulting first order ordinary differential equations are solved by a 4th order Runge Kutta Scheme (Gear, 1971).
The (parabolic) diffusion equation is solved by applying a Crank-Nicholson scheme (Richtmeyer and Morton, 1967). The solutions are obtained on a horizontal grid with 16 x 16 grid points (separation 20 km).

Based on typical variations in meteorological parameters with height and time, and the sensitivity of ground level concentrations to the emission height, we have fixed the vertical resolution to 50 m, up to the maximum height of 600 m (12 layers). The simplified equations (2.6) and (2.10) are solved by the same methods.

In the surface layer analytical solutions based on surface layer similarity are obtained. When it is assumed that no sources are present and that turbulent exchange of material is governed by the same mechanism as heat, the concentration profile is given by:

$$C(z) = C_o + \frac{0.74\ c_*}{k} \{\ln(z/z_o) - \psi_2(z/L)\} \qquad (2.17)$$

Businger, 1973). This profile should pass through the value obtained from the numerical solution at the lowest grid level (z = 25 m). This condition and the relation

$$V(z)\ C(z) = c_*\ u_* \big]_{z=25\ m}\ , \qquad (2.18)$$

where V(z) is derived from (2.12) and (2.13), determines the two unknowns C_o and c_* in (2.18).
More detailed information on the numerical procedures can be found in appendix B.

2.4. Meteorological Input.

2.4.1. Introduction

In the tranport equation (2.1) the horizontal wind field U, V and the diffusivity K_z have to be known, as functions of space and time. An operational air quality model should be based on meteorological data which are easily available i.e., without carrying out special measurements.
One of the major differences with most other current models is that the determination of the turbulence field is no longer based on stability classes (A-F), which are converted to the correct measure for the surface layer stability, the Obukhov length, by simple but ambiguous and thus unsatisfactory methods (e.g. Golder, 1972). Instead, estimates of L and u_* are based directly on an estimation of the heat flux and the wind speed (see also Fig. 3).

2.4.2. Observations.

Data from synoptic stations and radiosonde ascents are worldwide collected on a routine basis. Therefore, we will use these data to prepare the meteorolo

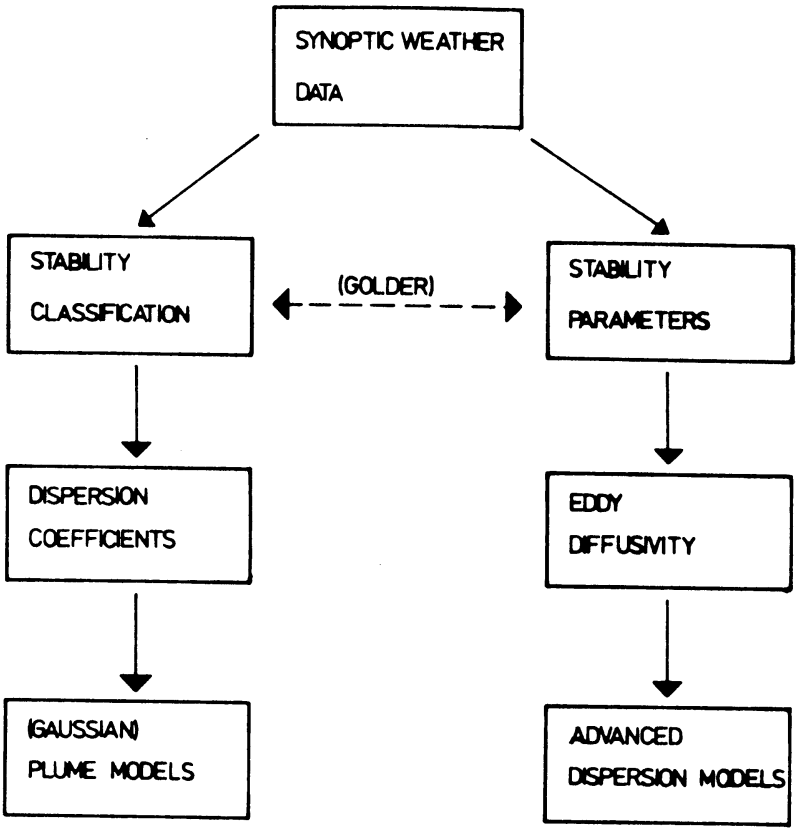

Fig. 3. Flow chart of the derivation of meteorological parameters for diffusion models.

gical input of the air pollution model. In addition other data may be used when they are available in a specific region. In tabel 2.I a review is given of meteorological observations used. The model requires hourly values of wind velocity and diffusivity, on a grid which was specified in section 2.3. In the appendix C is indicated how, with some use of our understanding of the atmospheric boundary layer, the desired input is derived from the observations.

2.4.3. The preparation of the meteorological input data

The two basic fields which are needed as input data are the wind and eddy diffusivity field. The mathematical procedure followed are given in appendix C. Here we will only resume the successive steps to obtain these fields.

Table 2.I. Meteorological observations in the considered region.

meteorological parameter	density[1]	
	at time intervals (hrs)	average distance (km)
precipitation	1-6	50
cloud cover	1	50
wind velocity (at 10 m)	1-3	50
temperature (surface)	1-3	50
pressure (surface)	1	50
upper air wind	6-12	200
upper air temperature	6-12	200
sodar data[2]	continuous	200
meteo tower data[2]	1/30-1	200

1) The data in this table are representative for Western Europe. Elsewhere they are usually more sparse.
2) Not routinely available.

a) Determination of the region of interest, choice of the gridsize, timestep etc.

b) Preparation of the inputfiles from routine data.
- Terrain properties (rougness, energy exchange and depostion properties).
- Synoptic station locations.
- (Hourly) synoptic reports.
- Aerological wind and temperature data.
- Tower and mast data (optional).

c) Extraction, inspection and correction of the desired data.

d) Interpolation of the basic fields.
- Wind field at observation height.
- Temperature field observation height.
- Pressure field observation height.
- Wind field at 1500 m height.
- (Optional tower wind field).

- Terrain properties
- Cloud cover.

e) Determination of turbulence parameters from the basic fields.

f) Construction of the final fields.

A series of (sometimes) timeconsuming computer programmes successively carry out the steps a-f. Because these procedures are neither standard nor streamlined, they are still pretty laborious and need a lot of looking after.

3. Some Results

3.1. Single source simulations

In order to test the accuracy of the numerical methods used, three simple cases are evaluated by the model. The cases are chosen such that also an analytical solution is available, with which the numerical solution can be compared. The third case is a simplification of an important meteorological process (fumigation).

3.1.1. Uniform conditions

The parameters used in the table are summarized in Table 3.I.

Table 3.I. Meteorological conditions for the numerical simulations.

			Case A	Case B
U	wind speed	(ms^{-1})	10	1
K_z	vertical eddy diffusivity	(m^2s^{-1})	5	$\begin{cases} 0.1 & (z<z_i) \\ 0 & (z>z_i) \end{cases}$
z_i	inversion height	(m)	∞	100
Q	source strength	(kgs^{-1})	1	1
H	source height	(m)	125	25

The basic equation (2.1), can be easily solved for the above cases.

Chemical transformation and deposition is excluded, so that S contains only the (single point) source,

$$S = Q\ \delta(x)\ \delta(y)\ \delta(z-H)\ , \tag{3.1}$$

where the location of the source is chosen in the origin (source height H and source strength Q). According to table 3.I equation (2.1) reduces in the stationnary, constant wind field and eddy diffusivity case to

$$U\ \partial C/\partial x = K_z\ \partial^2 C/\partial z^2 + S \tag{3.2}$$

Integration over y yields

$$U\ \partial C^y/\partial x = K_z \partial^2 C^y/\partial z^2 + S^y \tag{3.3}$$

where $C^y = \int_{-\infty}^{+\infty} C(x,y,z)dy$, etc.

Equation (3.3) is in fact the two-dimensional equivalent of (2.1). Dropping for simplicity the indices y, the analytical solution of (3.3) is

$$C = \frac{Q}{(2\pi)^{\frac{1}{2}}\ \sigma_z U}\ e^{-\frac{1}{2}\left(\frac{z-H}{\sigma_z}\right)^2}\ , \tag{3.4}$$

where $\sigma_z = (2K_z\ x/U)^{\frac{1}{2}}$. The solution in free (z-) space is given by (3.4). When one reflecting boundary at z = 0 is assumed the solution is:

$$C_1 = C(H) + C(-H)\ , \tag{3.5}$$

where C(H) is given by Eq. (3.4).

When another reflecting boundary at height z_i is assumed, an infinite amount of reflections should be included in the solution, and (3.4) should be replaced by:

$$C = \frac{Q}{(2\pi)^{\frac{1}{2}}\sigma_z U} \sum_{i=-\infty}^{j=+\infty} \left[\exp\left\{-\tfrac{1}{2}\left(\frac{z-H-2jz_i}{\sigma_z}\right)^2\right\} + \exp\left\{-\frac{z+H-2jz_i}{\sigma_z}\right\}^2\right] \tag{3.6}$$

The numerical values are compared with Eq. (3.6), where the series is cut off at $\|j\| = 2$.

The KNMI model is designed such, that it requires as input a mixed-layer or inversion height. The maximum value of this parameter is 600 m (when the actual mixed layer height exceeds this value, Eq. (3.1) is modified (see section 2.2).

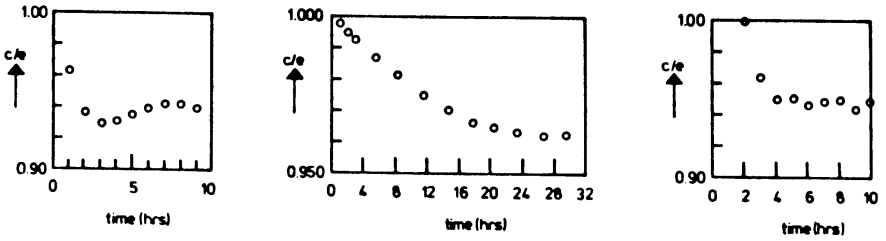

Fig. 4. Mass conservation tests. (a) case A; (b) case B; (c) the fumigation case. The ratio c/e denotes the integrated concentration, $\int_{vol} C\ dv$ divided by the emitted amount of material, e.

Another particular property of the model is that cross-wind diffusion is neglected so that we will present in the following cases cross-wind integrated concentrations only.

Case A.

A first test was done on mass conservation. In Fig. 4 the ratio of the total

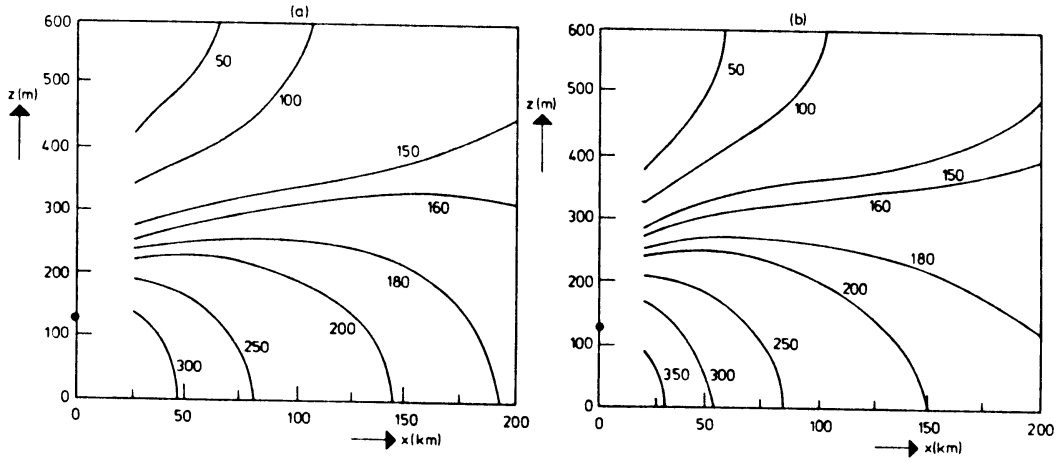

Fig. 5. Numerical (a) and analytical (b) results for case A, presented in a vertical cross-section through the source (o). Isopleths denote the concentration in mgm^{-2}.

mass present in the grid and the emitted mass is compared for the first few hours after the start of the run. We observe that a small reduction in material occurs which may be estimated to be 6 % after 9 hrs. This reduction is a consequence of the used numerical procedure. It is not considered very serious for practical applications. In Fig. 5 an x-z cross-section through the plume-axis is presented and compared with the analytical one.
Finally some profiles are depicted in Fig. 6.

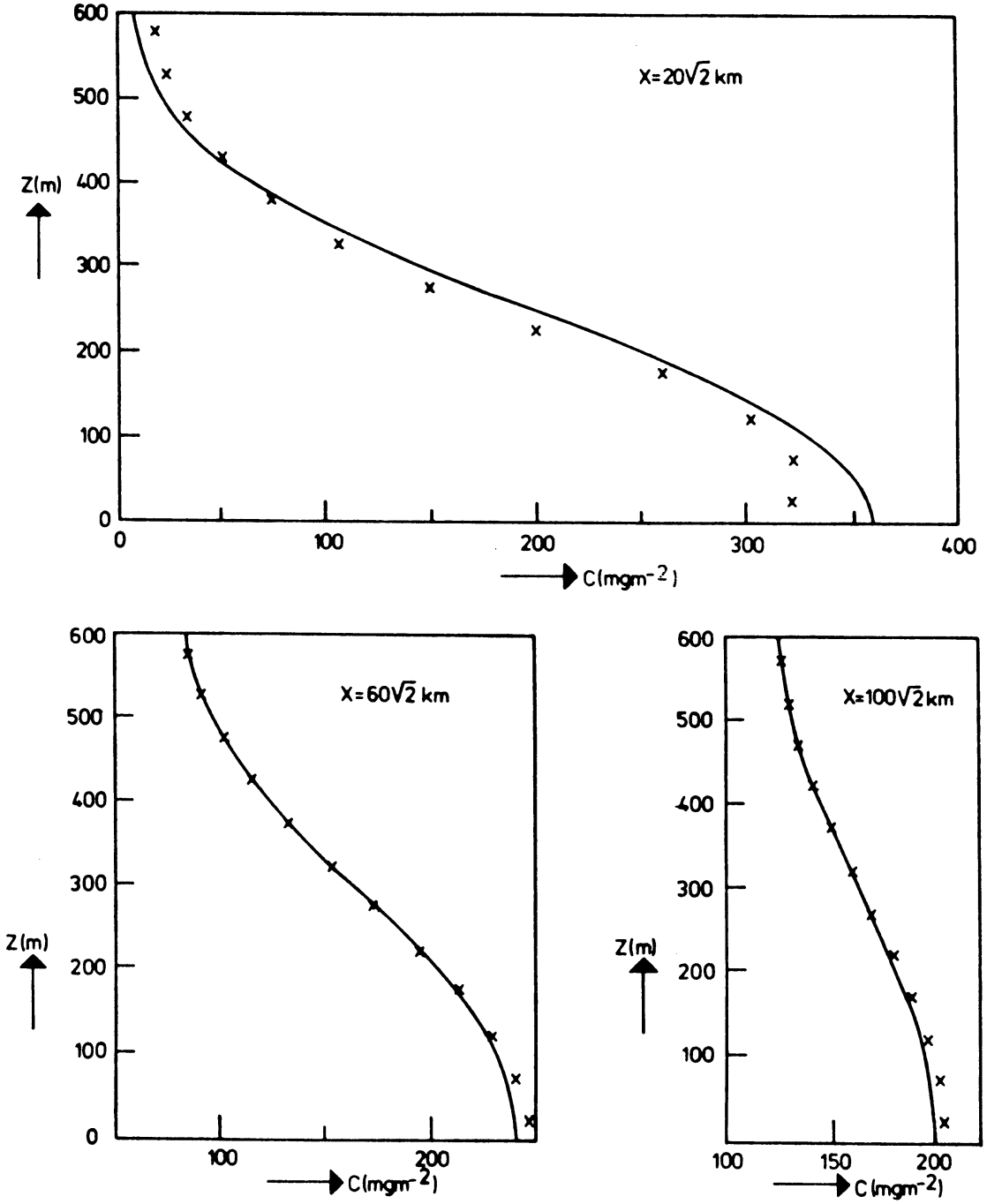

Fig. 6. Case A. Vertical concentration profiles at three downwind distances. The solid lines indicate the analytical solution.

Case B.

Also for this case first the mass conservation was tested (Fig. 4). We observe also mass annihilation which amounts to 4 % after a 36 hr simulation.
We compared the numerical solution of the 36th hour with the analytical steady state solution. The results are given in Table 3.II. It appears that both solutions tend to a homogeneous distribution after ~ 50 km down-wind distance.

Table 3.II. Cross-wind integrated concentrations (gm^{-2}) for case B.

		downwind distance x(km)		
		$20\sqrt{2}$	$40\sqrt{2}$	$60\sqrt{2}$
z = 75 m	analytical	9.39	9.96	10.00
	numerical	8.09	9.67	9.96
z = 25 m	analytical	10.61	10.04	10.00
	numerical	10.65	9.98	9.98

It should be noted here that it would have been natural to scale down the vertical grid-mesh to solve case B. However, the described conditions are met in practice, and it is more useful to know how the unmodified model behaves in these extremely stable conditions.

3.1.2. Fumigation.

Here we describe the case where a point source initially emits above the mixed-layer. The mixed-layer is steadily rising, thus simulating an inversion break-up during the morning hours. The parameters used for this simulation are given in table 3.III.
The mass conservation test was also done (Fig. 4). In Fig. 7 the cross-wind integrated concentrations are given for t = 3 and 4 hr. For t > 5 the mixed-layer height exceeds 600 m. Our model jumps then automatically to another, faster numerical routine, where it is assumed that the vertical concentration distribution is homogeneous.

This concentration distribution is given at t = 6 and 12 hrs, as a function of down wind distance in Fig. 8. An approximate analytical solution for this case is presented in Appendix D.

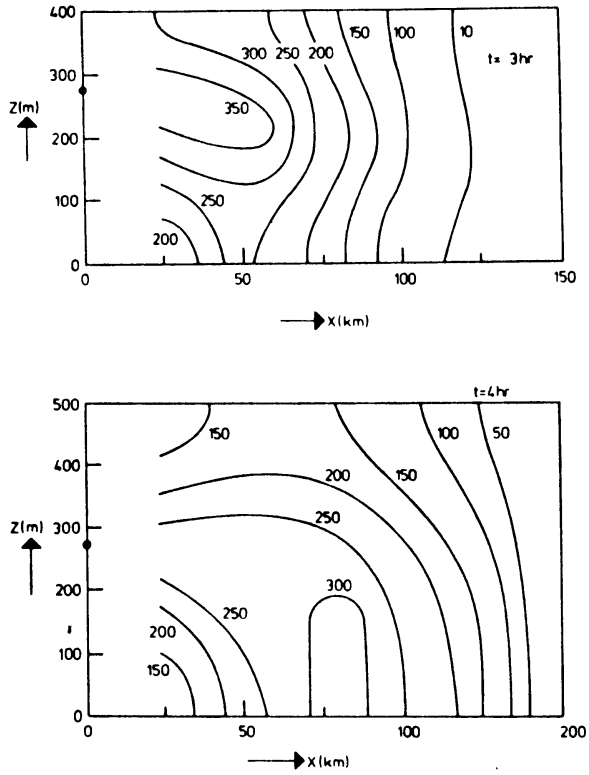

Fig. 7. Fumigation case after 3 and 4 hr respectively. The source is indicated by the dot. Concentrations are in mgm^{-2}.

Table 3.III. Meteorological conditions for the fumigation.

$U = 10\ ms^{-1}$
$K_z = \begin{cases} z_i/100\ m^2s^{-1} & z < z_i \\ 0 & z > z_i \end{cases}$
$z_i = 100(t+1)\ m, \quad 0 \leq t \leq 12$
$Q = 1\ kgs^{-1}$
$H = 300\ m$

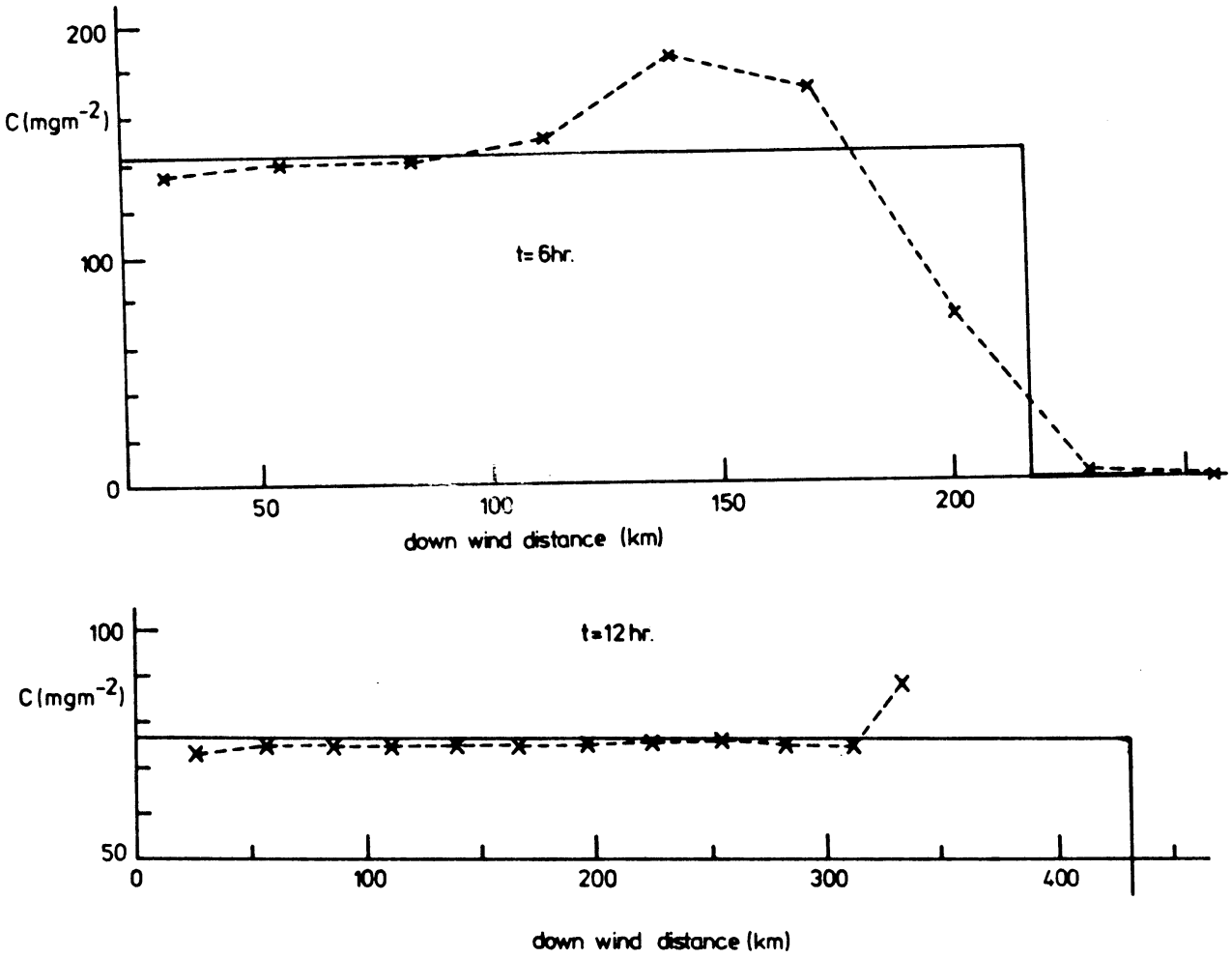

Fig. 8. Fumigation case after 6 and 12 hr respectively. Because the mixing height exceeds 600 m the model equation (2.10) applies, resulting in average mixed layer values (mgm^{-2}). The solid lines depict the exact solution of Eq. (2.10).

3.2. A Simulation of the episode 29-30 May 1978: a test case.

After the simple numerical tests, real meteorological fields were used. Meteorological data were prepared for (see appendix C) the period 29 May 1978, 00.00 GMT to 30 May 1978, 11.00 GMT. These days were characterised by sunny weather. A strong stationnary anticyclone over Scandinavia maintained a weak and steady (north)easterly flow. The output consisted of hourly horizontal wind and eddy diffusivity fields over twelve equidistant layers, varying in height from 50 to 600 m.

The model was run with these data and the initial conditions that the concentration was zero. The influx of pollutant at the upwind boundary is neglected. The emissions in the area were estimated from a sulphur emission inventory

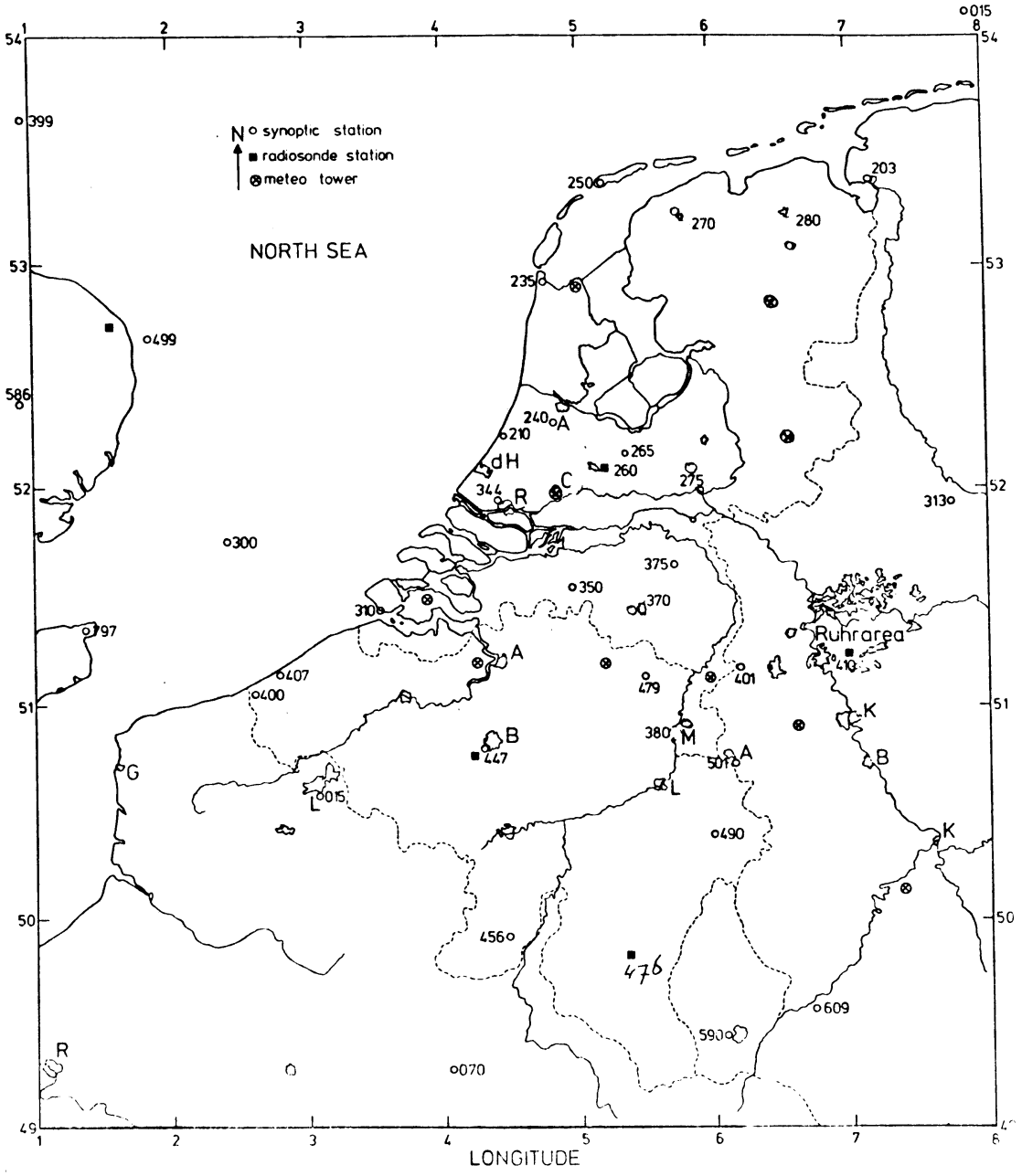

Fig. 9. Locations of synoptic and radiosonde stations, and meteorological towers in the model region.

made in 1977 (Van Egmond and Kesseboom, 1982 and TNO, 1979). The numerical simulations were carried out in a sub-region ranging from 1°-6° Eastern Longitude and from 49.5°-52.5° Northern Latitude (cf. Fig. 9). The following case studies were carried out:

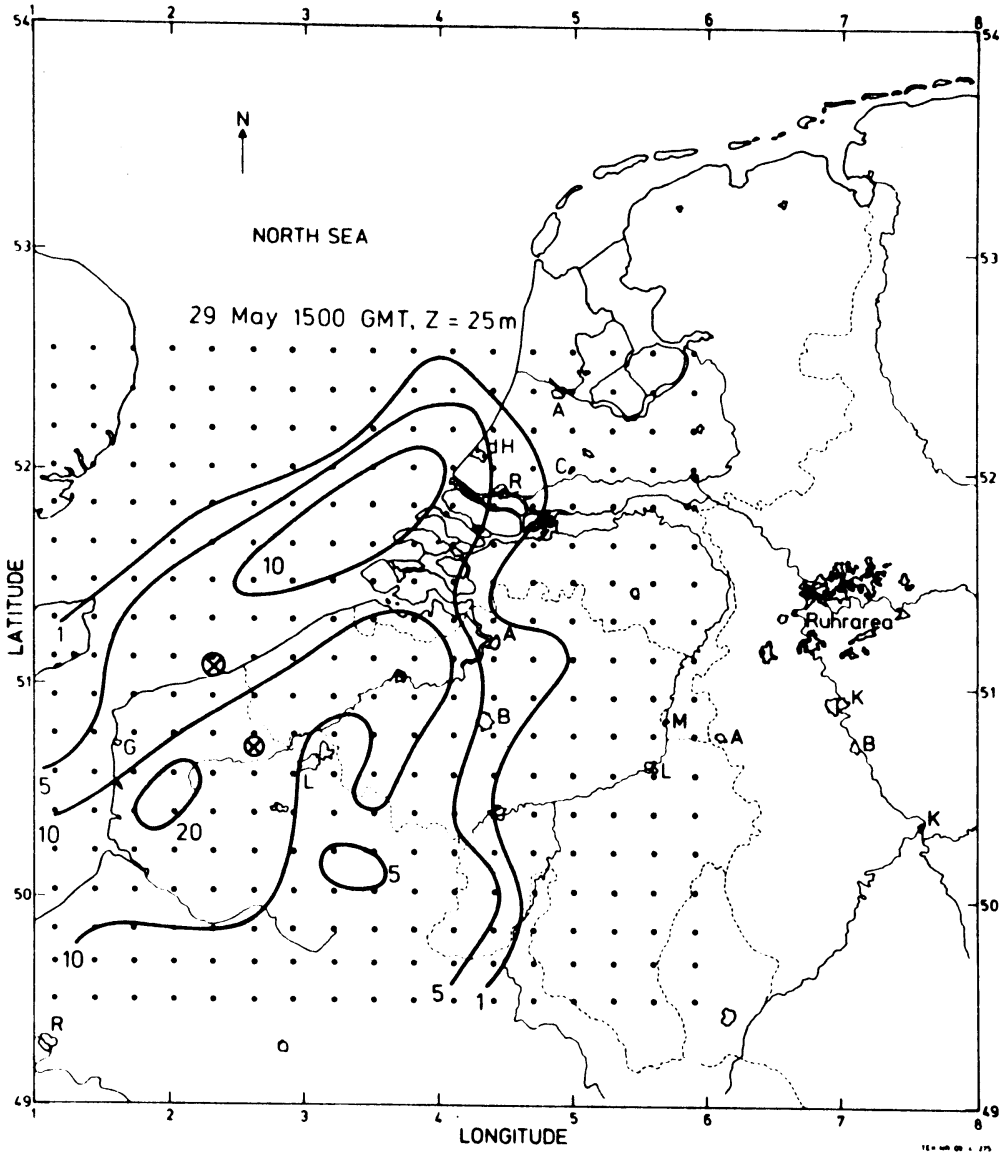

Fig. 10. SO_2 Concentration distribution $[\mu gm^{-3}]$ at 25 m height, on 29 May 1978, 15.00 GMT. Meteorological data are evaluated in the whole region. The dotted array indicates the computational grid which can be shifted (or enlarged) over the shown region. The receptor points (see text) are indicated by ⊗.

(i) a run with high and low source emissions, including dry deposition,

(ii) a run with the same emission, excluding dry deposition and

(iii) a run where surface source emissions are excluded, in order to study the effect of high source emissions only.

3.2.1. All sources, dry deposition included.

The run started at 29 May, 00.00 GMT. Fig. 10 shows the concentration distribution at 15.00 GMT. The down wind plumes of the large industrial areas near Rotterdam and Antwerpen are clearly visible. Evidently surface sources in Western Belgium and the North-Western part of France produce a local maximum of ~ 20 μgm^{-3} in France.

During the night (Fig. 11) a build-up of concentrations occurs, mainly due to local surface sources.

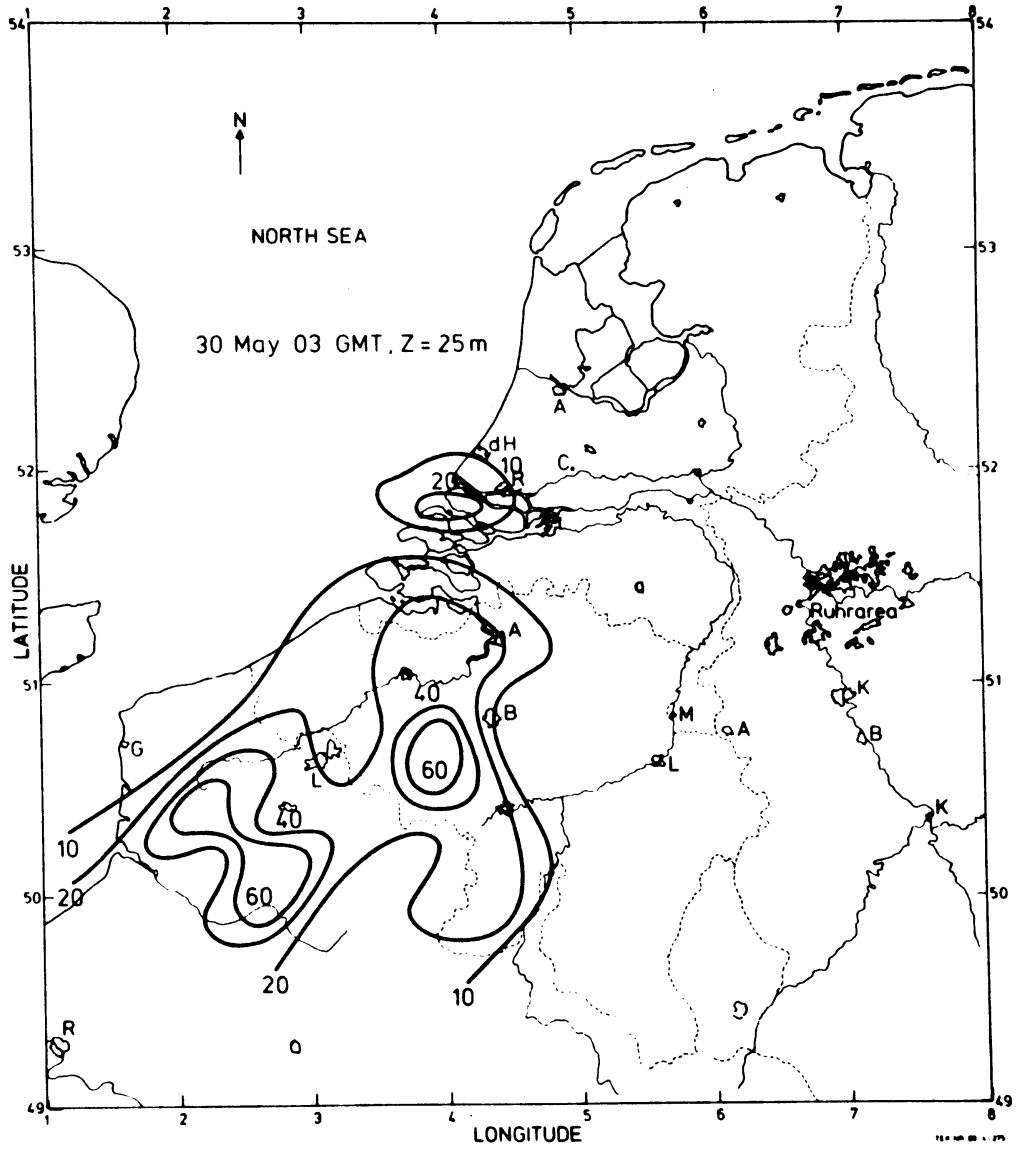

Fig. 11. As Fig. 10, 30 May 1978, 0300 GMT.

At fixed locations downwind of the major source locations (cf. Fig. 12) the diurnal cycle of the concentration was determined. A rural location at the coast, and a more urban, mainly surface source influenced location were selected. We observe in Fig. 12 that the surface sources (73% of the total emission) dominate in the concentration distribution. During daytime the concentration distribution is homogeneous; when, however, during the night the stability increases a concentration gradient develops. The maximum values occur at 25 m height, which is the standard height for all surface source emissions.

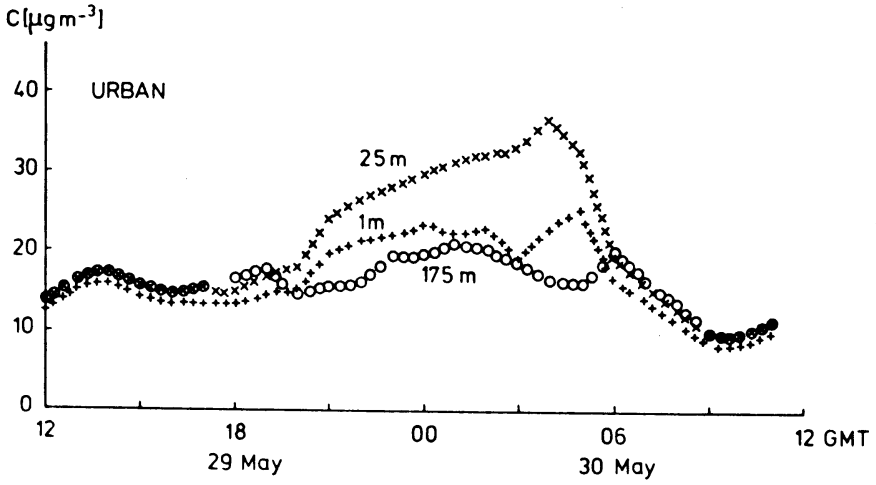

Fig. 12. Diurnal variation of the SO_2-concentration at 1, 25 and 175 m height. The concentrations were evaluated, using the full emission inventory within the computational area only (cf. fig. 10).

3.2.2. All sources, without dry deposition.

In order to study the effects of dry deposition the run was repeated with the dry deposition "switched off". The effect on the concentration at 25 m is considerable, and amounts to a factor of two (Fig. 13). At 75 and 125 m the decrease in concentration by the deposition process is somewhat smaller. The concentrations at 1 m height were also evaluted. In the case with dry depositon this was done by application of the relation

$$C(1) = C(25)/[1 + V_g \cdot r(25,1)] , \qquad (3.7)$$

where C(1) and C(25) respectively denote the concentrations at 1 and 25 m, and r(25,1) is given by (2.13). In the zero deposition case the 1 m concentration was obtained by simple extrapolation of the two lowest grid values, using the

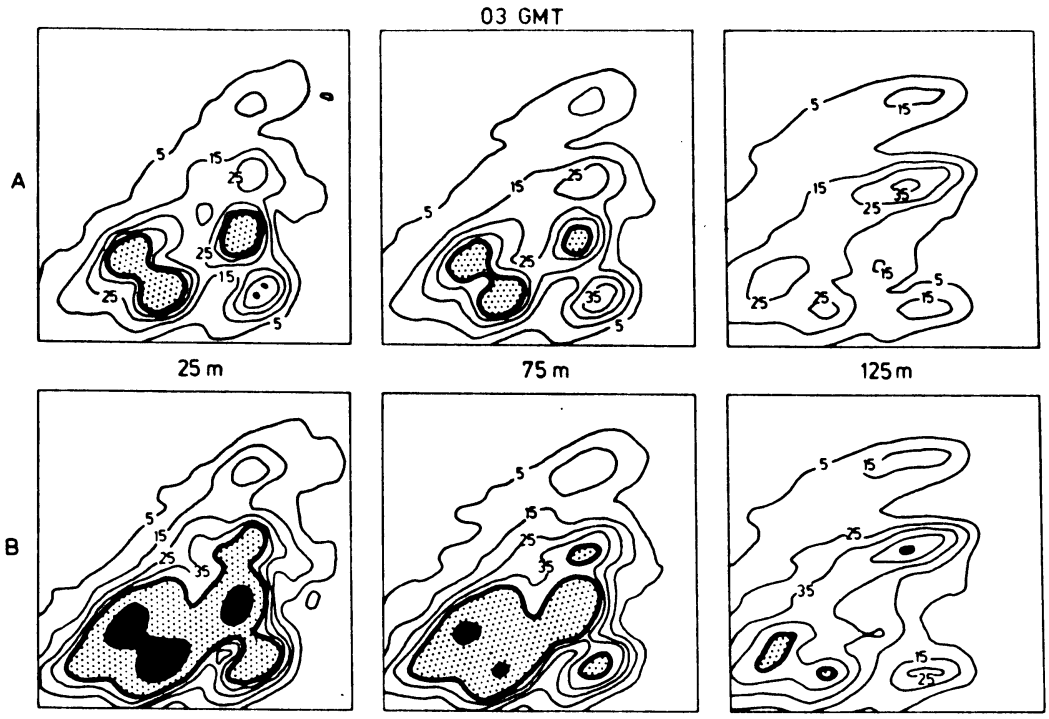

Fig. 13. Concentration pattern at three heights on 30 May 0300 GMT; (a) evaluated with, and (b), without dry deposition. Isopleths are given for 5, 15, 25 ... μgm^{-3}.

condition $\partial C/\partial z = 0$, at $z = 0$. The results are given in Fig. 14. We observe that the differences in well-mixed conditions amounts to 1.5 - 2. In stable nighttime conditions the differences may be a factor three or more, which indicates the importance of the inclusion of the deposition process even on these transport scales. This result is obtained from one receptor point only. We hope to give a more detailed analysis of the deposition over the whole area and in a variety of meteorological situations in the near future.

3.2.3. High source emission only.

To study the dispersion of high source emission (> 25 m) the surface emissions were "switched of", and a new simulation was started. As expected, concentrations at higher levels are highest in stable conditions (Fig. 15). We further note a fair resemblence with observations of the diurnal variations at Cabauw (Van Dop et al., 1980), which has a similar position with respect to surrounding high sources as the receptor point for the present simulation. We also mark the fumigation episode (Fig. 15) during the early morning hours, where within a few hours the surface layer concentrations increase by a factor 3.

Figure 16 shows some vertical profiles at the urban receptor location. We

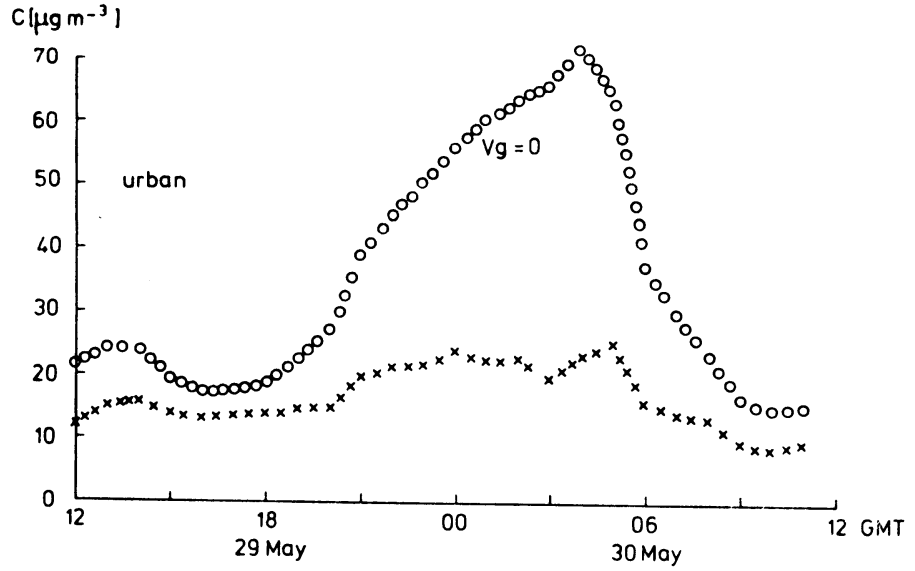

Fig. 14. Diurnal variation at the urban receptor point (z = 1 m) with (x) and without (o) dry deposition.

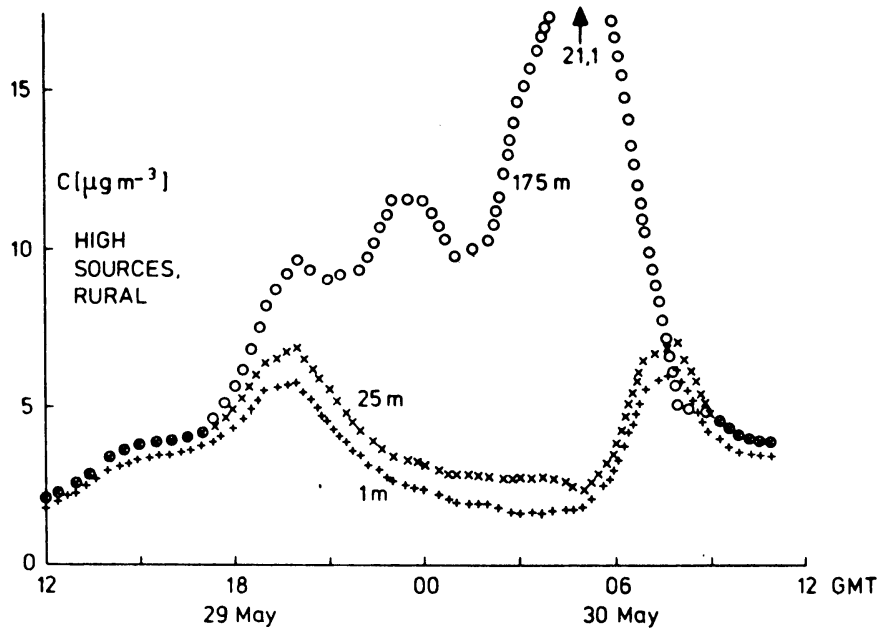

Fig. 15. Diurnal variation in the concentrations at 1, 25 and 175 m due to emissions from high sources only (rural receptor point).

observe that the concentrations at this location are strongly dominated by surface sources. It is also shown that the atmospheric stability is nicely reflected in the concentration profiles: during nighttime the concentration maximum is at the height where the major sources are, while in unstable conditions the pollutant is well-mixed in the depicted layer. Note that, though the elevated source fraction is .27, their contribution to ground level concentration (1 m) is 0.15 or less.

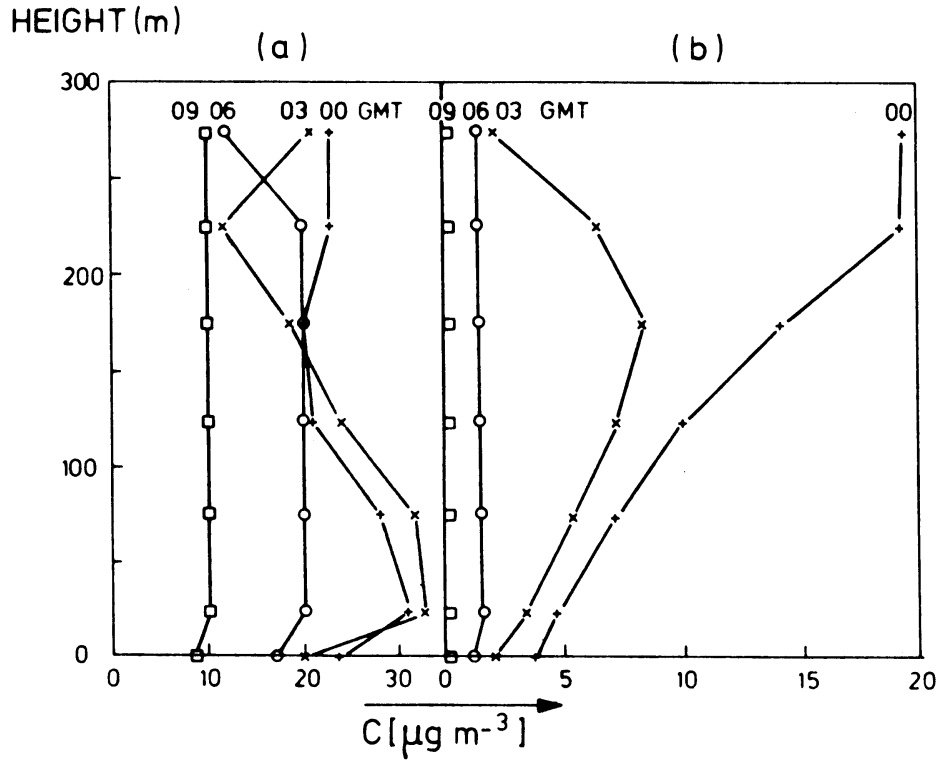

Fig. 16. Vertical profiles at the urban receptor point (30 May 1978 00, 03, 06 and 09 GMT. (a) All sources and (b) high sources only (note the difference in scale along the horizontal axis).

Summary

A diagnostic mesoscale air pollution model is described and some results are given. Though the operational use of the model requires further testing and comparison with observed concentrations we may conclude that:

(1) The model assumptions lead to realistic concentration fields, i.e. patterns which are in qualitative accordance with atmospheric stability: a reasonably homogeneous vertical concentration distribution during unstable daytime conditions, and (strongly) varying concentration distribution during the night.

(2) Due to the high vertical resolution (50 m up to 600 m) we are able to introduce elevated emissions at the proper heights. The preliminary results show that a strong relation exists between the vertical distribution of the sources and the concentration, especially in stable conditions.

(3) The influence of the dry deposition on the concentration pattern at ground level is considerable. A more careful analysis for other receptor points still should be carried out. Nevertheless, the model provides in principle

the possibility to calculate deposited amounts of pollutant material, when the deposition velocity is known.

(4) The fumigation process - which is often observed in diurnal ground level concentration data - is well simulated by the model calculations.

(5) The complexity of the model considered the computer time requirements are moderate: ≃ 24 hr run on a Burroughs 6800 computer takes approximately 30 minutes CPU time. The computer time required for the preparation of the meteorological data, however, should be added to that.

(6) At this stage no attempt was made to compare the model data with measurements in the region. Uncertainties in the emission data and air pollution inflow from outside the model region make such a comparison highly speculative. The authors, however, recognise the necessity of some measure of the quality and performance of the described model. We therefore decided to cooperate in a model intercomparison study initiated by NATO-CCMS. This study is devoted largely to the performance of meso scale air pollution models in practical situations. We hope to report from this study by the end of 1983.

Acknowledgement

This work was sponsored by the Ministry of Health and Environmental Protection.

References

Aalst, R.M. van and Bergsma, F. (1981). Removal and transformation processes in the atmosphere with respect to SO_2 and NO_x. NATO-CCMS Report No. 127, pp. 50.

Adam, J. (1977). Highly accurate compact implicit methods and boundary conditions. Journal of Computational Physics, 24, 10-22.

Briggs, G.A. (1971). Some recent analyses of plume rise observation. Procs. 2nd international clean air congress, 6-11 December 1970. Acad. Press (New York), 1029-1032.

Brost, R.A.and Wyngaard, J.C. (1978). A model study of the stably stratified planetary boundary. J. Atmos. Sci. 35, 1427-1440.

Bruin, H.A.R. de and Holtslag, A.A.M. (1981). A simple parameterization of the fluxes of sensible and latent heat during daytime compared with the Penman-Monteith concept. Submitted to J. Appl. Meteor. (Preprint available)

Businger, J.A. (1973). In: Workshop on micrometeorology, Haugen, D.A. (Ed.) American Meteorological Society.

Cats, G.J. (1980). Analysis of surface wind and its gradient in a mesoscale wind observation network, Mon. Wea. Rev., 108, 1100-1107.

Christensen, O. and Prahm, L. (1976). A pseudospectral model for dispersion of atmospheric pollutants, Journal of Applied Meteorology, 15, 1284-1294.

Crowley, W.P. (1967). Second-order numerical advection. J. Comp. Phys., 1, 471-484.

Crowley, W.P. (1968). Numerical advection experiments. Mon. Wea. Rev., 96, 1-11.

Dop, H. van and Haan, B.J. de (1981). A mesoscale air pollution transport model: outline and preliminary results. Procs. of the 12th NATO/CCMS International Technical meeting on air pollution modeling and its application, Palo Alto, August 25-28, xxxxx.

Dop, H. van, Ridder, T.B. and Tonkelaar, J.F. den (1980a). Sulphur dioxide measurements on the 213 m tower at Cabauw, the Netherlands, Atmos. Environment, 14, 933-945.

Dop, H. van, Haan, B.J. de, and Cats, G.J. (1980b). Meteorological input for a three dimensional medium range air quality model. Procs. of the 11th ITM, NATO-CCMS, 24-27 November, Amsterdam, (1981), 64-72.

Dop, H. van (1983). Terrain classification and derived meteorological parameters for interregional transport models. Submitted to Atmospheric Environment.

Driedonks, A.G.M. (1981). Dynamics of the well-mixed atmospheric boundary layer. Thesis, Royal Netherlands Meteorological Institute (KNMI), 3730 AE De Bilt, pp. 189.

Egmond, N.D. van, and H. Kesseboom (1982). Mesoscale air pollution dispersion models; A: Eulerian Grid-Model. Submitted to Atmospheric Environment.

Endlich, R.M. (1967). An iterative method for altering the kinematic properties of windfields, Journ. Appl. Meteor., 6, 837-844.

Fisher,B.E.A. (1982). The transport and removal mechanism of sulphur dioxide in a rain system, Atmospheric Environment 16,775-783.

Forester, C.K.(1977). Higher order monotonic convective difference schemes, J. Compu. Phys., 23, 1-22.

Fox, D.G. and Orszag, S.H (1973). Pseudospectral approximation to two dimensional turbulence, J. Comp. Phys., 11, 612-619.

Gadd, A.J. (980). Two refinements of the split explicit integration scheme, Quarterly Journal of the Royal Meteorological Society, 108, 215-220.

Gadd, A.J. (1978). A numerical advection scheme with small phase speed errors, Quarterly Journal of the Royal Meteorological Society, 104, 583-594.

Garland, J.A. (1979). Dry deposition of gaseous pollutants Procs. of the WMO Sympsoium on the long range transport of pollutants and its relation to general circulation including stratospheric/tropospheric exchange processes, Sofia 1-5 October, WMO-report No. 538.

Gazdag, J. (1973). Numerical convective schemes based on accurate computation of space derivatives, Journal of Computational Physics, 13, 100-113.

Gear, C.W. (1971). Numerical initial value problems in ordinary differential equations. Prentice Hall, Inc., New Jersey, pp. 253.

Golder, D. (1972). Relations among stability parameters in the surface layer, Boundary-Layer Meteor., 3, 47-58.

Gottlieb, D. and Orszag, A. (1977). Numerical analysis of spectral methods: theory and applications. Society for industrial and applied mathematics, Philadelphia.

Haan, B.J. de (1980). A comparison of finite difference schemes, describing the two-dimensional advection equation. Preprint of the procs. of the 11th ITM, Nato-CCMS, Amsterdam, 24-27, November 1980. Pennsylvania 19103, pp. 172.

Holtslag, A.A.M, de Bruin H.A.R., Van Ulden, A.P. (1981). Estimation of the sensible heat flux from standard meteorological data for stability calculations during daytime. In: "Air Pollution Modelling and its Application I, C. de Wispelaere, (ed.), Plenum, New York.

Holtslag, A.A.M., and Van Ulden, A.P. (1982). Simple estimates of nighttime surface fluxes from routine weather data. Scientific Report W.R. 82-4, KNMI, De Bilt.

Hout, K.D. van den and H. van Dop (1981). State of the art of interregional modelling. NATO-CCMS Report no. 126, pp. 73.

Lamb, R.G. (1982), in: Atmospheric Turbulence and Air Pollution Modelling. F.T.M. Nieuwstadt and H. van Dop (ed.), R. Reidel, Dordrecht (1982), Ch. 5.

Molenkamp, C.R. (1968). Accuracy of finite difference methods applied to the advection equation, J. Appl. Meteor., 7, 160-167.

Nieuwstadt, F.T.M. (1977). The dispersion of pollutants over a water surface. Proceedings of the 8th International Technical Meeting on air pollution and its application, September 20-23, 1977.

Nieuwstadt, F.T.M., and B.J. de Haan (1981a). An analytic solution of the one-dimensional diffusion equation in a non-stationnary boundary layer with an application to inversion rise fumigation. Atmos. Environ., 15, 845-851.

Nieuwstadt, F.T.M. (1981a). The steady-state and resistance laws of the nocturnal boundary layer: theory compared with observations. Bound. Layer Meteor. 20, 003-017.

Nieuwstadt, F.T.M. (1981b). The nocturnal boundary layer. Thesis, Royal Netherlands Meteorological Institute (KNMI), 3730 AE De Bilt.

Orszag, S.A. (1971). Numerical simulation of incompressible flows within simple boundaries: accuracy. J. Fluid Mech., vol. 49, part 1, 75-112.

Pasquill, F. (1974). Atmospheric Diffusion, Wiley, New York, London, (2nd edition), pp. 429.

Praagman, N. (1979). Numerical solution of the shallow water equations by a finite element method, Dissertation at the University of Delft, the Netherlands.

Praagman, N. and Segal, A. (1974). On the solution of systems of linear ordinary differential equations. Initial value problems. NA report 11, Technical University Delft, 1974.

Purnell, D.K. (1976). Solution of the advective equation upstream interpolation with a cubic spline, Monthly Weather Review, 104, 42-48.

Richtmeyer, R.D., and Morton, K.D. (1967). Difference methods for critical value problems. Interscience Publishers, New York, pp.405.

Sehmel, L.A. (1980). Particle and gas dry deposition: a review. Atmospheric Environment, 9, 983-1011.

Smith, F.B. and Carson, D.J. (1977). Some thoughts on the specification of the boundary layer relevant to numerical modelling. Bound.-Layer Meteor. 12, 307-330

Tennekes, H. (1973). A model for the dynamics of the inversion above a convective boundary layer. J. Atmos. Sci. 30, 558-567.

Thom, A.S. (1972). Momentum, mass and heat exchange of vegetation. Quart. J.R. Met. Soc., 98, 124-134.

TNO(1979). Rekensyteem luchtverontreiniging, Schoenmakerstraat, Delft, The Netherlands

Venkatram, A. (1980). Estimation of turbulence velocity scales in the stable and the unstable boundary layer for dispersion applications. Procs. of the 11th ITM, Nato/CCMS, Amsterdam, 24-27 November, 169-179, Plenum Press, New York.

Wengle, H., and Seinfeld, J.H. (1978). Pseudospectral solution of atmospheric diffusion problems, J. Comp. Phys., 26, 87-106.

Wesseling, P. (1972). On the construction of accurate difference schemes for hyperbolic partial differential equations, Journal of Engineering Mathematics, 7, 19-31.

Wieringa, J. (1976). An objective exposure correction method for average wind speeds measured at a sheltered location. Quart. J.R. Met. Soc., 102, 241-253.

Wieringa, J. (1980a). Estimation of mesoscale and local roughness for atmospheric transport modeling. Procs. of the 11th NATO/CCMS international technical meeting on air pollution modeling and its application, 279-295,

Wieringa, J. (1980b). Respresentativeness of wind observations at airports. Bull. Am. Meteor. Soc., 61, 962-971.

Young, J.W.S. (1981). Evaluation of model performance in support of the Canada-USA air pollution treaty overview. Procs. 12th ITM, NATO-CCMS, Palo Alto, 21-28 August, 1982, Plenum Press, New York,1982,

APPENDIX A: Terrain classification and derived meteorological parameters for interregional transport models.

The earth's surface plays an important role in the determination of the above parameters. Also deposition - another important topic in air pollution modelling - strongly depends on surface properties. Therefore, an adequate description of the surface characteristics seems to be a necessary requirement in the design of modern atmospheric transport models. Terrain features which should be incorporated are surface roughness, physical and chemical properties.

The surface roughness determines the shape of the wind profile in the surface layer. Moreover, it plays an important role in the generation of turbulence, and thus influences diffusion. Also the rate of deposition is affected by the turbulence intensity near the surface (Thom, 1972).

The relevant physical properties of the soil consist of its ability to transform incoming radiation into sensible heat flux. The latter quantity determines to a large extent whether the atmospheric boundary layer is stable or unstable. The nocturnal inversion height as well as the daytime mixed-layer height - which play an important role in atmospheric dispersion - are closely related to the sensible heat flux.

The chemical properties of the soil determine the uptake of pollutants from the air. A generally accepted method to describe the uptake is the deposition velocity concept (Thom, 1972). The deposition velocity is determined by the combination of the chemical properties of the soil and the pollutant. A recent review for various types of soil and pollutants is given by Sehmel (1980).

All the above mentioned terrain properties can be estimated by careful inspection of the terrain in the region under investigation. The spatial resolution corresponds to the resolution of the dispersion model (gridsize 20x20 km^2).

This means that terrain characteristics which are averaged over squares of approximately that size are needed.

In this appendix we will indicate how from data depicted on topographical maps the relevant terrain properties can be derived. The emphasis will be on the determination of the surface roughness, but the determination of some other properties will also be discussed.

1. The use of land maps for terrain classification.

Topographical description is a typical national activity. For most countries in Western Europe detailed topographical maps are available for a variety of purposes. The map scales range from $1:10^3$ to $1:10^6$. They vary accordingly in their ability to resolve the smallest details. For the determination of average terrain properties from land maps on squares of 20x20 km^2, one should choose a scale which is small enough to reveal enough details of the terrain, and, on the other hand large enough not to be overwhelmed with unimportant details. We decided to use land maps with a scale of 1:250.000*. The area considered consisted of the Benelux, the Northern par of France, the Western part of the Federal Republic of Germany (FRG), and the most Eastern part of the United Kingdom (UK), covering an area from 49°-54° N and 1°-8° E.
For reasons of simplicity areas of 10'x10' (approximately 10x20 km^2) were analyzed. This was done by estimating (by eye) the three largest fractions of indicated terrain features in that particular square.
The first fraction was estimated to cover 67% of the total area, the second 22% and the third 11%. The common features revealed on all maps were: roads, buildings, wood, water features and relief. Open field is mostly indicated by the absence of the other features. Some maps reveal more details than other ones (e.g., terrain with low crops, or scattered trees). Percentages were tabulated of the following categories:

1. water surface
2. open field
3. field with scattered trees and hedges
4. forest
5. buildings
6. roads, railways.

From each 10'x10' area the most important terrain features were selected. Also the average height and average height difference of the area was noted. These data were coded and dumped on tape labeled with their coordinates.

* For the Federal Republic of Germany only maps on a scale 1:200.000 were available.

2. The specification of surface properties.

Three surface characteristics of importance in interregional modelling will be considered below: energy exchange, roughness and depostion.
Because the region considered is relatively flat orographic effects will be neglected.
It is not our intent to go into the details of the physical and chemical processes at the surface. Some examples will be given of how these processes can be modeled with some knowledge of the terrain. However, both terrain description and physico-chemical modelling can be made as sophisticated as desired.

3. The energy exchange.

Atmospheric stability depends strongly on the energy exchange at the surface. It depends directly on the sensible heat flux. It is determined by a variety of quantities. In a quasi-stationary situation, for daytime conditions over land, H is given by:

$$H = \frac{(1-\alpha)S + \gamma}{S + \gamma} (Q^* - G) - \beta \ , \qquad (A.1)$$

(see appendix C). The net radiation is denoted by Q^*, and soil heat flux by G. The soil heat flux is taken equal to 10% of the net radiation. The temperature dependent functions S and γ are given in appendix C,Eq.(C11). Observations at Cabauw indicate that $\alpha = 1$ and $\beta = 20$ Wm^{-2} (Holtslag et al., 1981). These values are considered representative for the terrain categories 2-4. for the terrain categories 5 and 6 $H \simeq Q^* - G$, so that α and β are both set to zero. When in a 10'x10' area terrain categories are encountered belonging to both the categories 2-4 and 5 or 6 (see Section 2), α and β are determined by linear interpolation between the values (0, 1) and (0, 20) respectively according to the cover percentage. This means that during constant atmospheric conditions the change in H over various terrain may be of the order of H itself (cf. equation (A.1).
Over a water surface (category 1) and during nighttime other procedures are followed to determine the sensible heat flux and atmospheric stability (Nieuwstadt, 1977 and Venkatram, 1980), in which surface characteristics are not relevant.

4. Surface roughness

The specification of the surface roughness is of particular importance because it influences both the horizontal wind velocity (transport) and the atmospheric turbulent intensity (diffusion). In Table A.I we present some values of the roughness length, z_o. It varies by orders of magnitude over

Table A.I. Roughness length for some terrain categories, according to Wieringa, 1980a, b.

Terrain category	z_o[m]	C_d*)(10) x 10^3
water surface	0.0005	1.7
open field	0.03	5
open field with scattered trees and hedges	0.25	12
roads/railways	0.50	19
wood	1.00	32
buildings	2.00	65

*) According to Eq. (A.2).

different kinds of terrain. It is possible to determine the roughness of a homogeneous surface, but to estimate the roughness of areas with varying surface structure (Wieringa, 1980a) is next to impossible. For example, the surface roughness of an area consisting of - 50% forest and 50% open field is more likely to be close to that of the forest or even slightly larger, because the change in terrain itself contributes to the roughness. As a rule of thumb one may state that an area with varying surface structure tends to attain the roughness which corresponds to the roughest elements in the area.
Furthermore if the area considered, is large, it is likely that rough terrain categories are encountered. Larger areas thus tend to have larger roughness lengths. This should be kept in mind when average roughness values are assigned to 10'x10' areas.
Another aspect in determining an average roughness is that z_o varies by 5

orders of magnitude, so that linearly averaging does not make much sense. Therefore, we take average drag coefficients (see Smith and Carson, (1977)**. In order not to be harrassed by stability effects we use the following relation between z_o and the 10 m drag coefficient, $C_d(10)$:

$$C_d(10) = (k/\ln(10/z_o))^2 \ . \qquad (A.2)$$

As already was stated in the previous section, from each 10'x10' area the three most important (by occurrence) terrain features were noticed, by visual inspection. In order to determine the average roughness each feature should be given a certain weight according to a.o. the relative cover. In view of the above considerations, however, a reasoned choice can hardly be made. We therefore varied the weighting factors tentatively such that in very well known terrain reasonable values were obtained. This resulted in modified

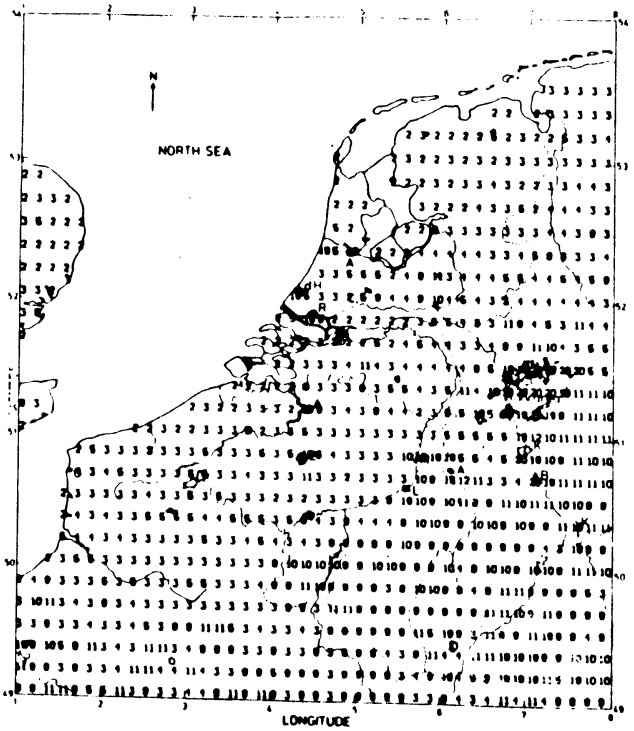

Fig. 17. The rougness length (in dm) averaged over rectangles of 10'x10' arcminutes (~ 10 x 20 km^2).

**) Hereafter referred to as SC.

values of 0.85, 0.125 and 0.025 for the weighting factors f_1, f_2 and f_3 respectively, so that a representative drag coefficent, C_d, for a 10'x10' area could be determined from:

$$C_d = f_1 C_{d1} + f_2 C_{d2} + f_3 C_{d3}. \qquad (A.3)$$

In Eq. (A.3), C_{d1} denotes the drag coefficient of the dominant terrain type, C_{d2} the next important,, and C_{d3} the least extensive terrain category. The resulting values of C_d are converted to z_o by equation (A.2.) and shown in Figure 17. The large variation in z_o results in a similar, correlated pattern

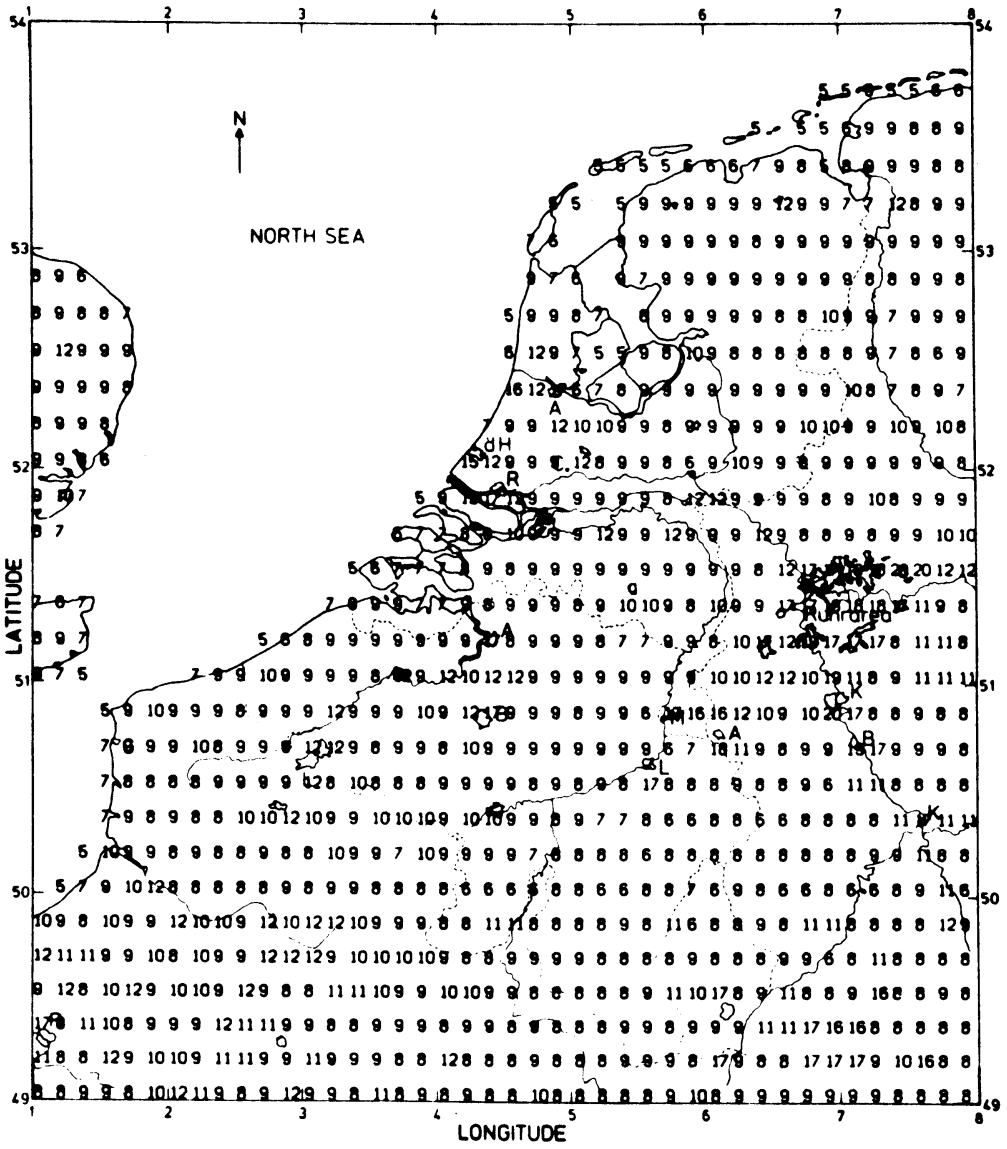

Fig. 18. As fig. 17 for the deposition velocity.

of the friction velocity in the area (Van Dop and De Haan, 1981). An example is given in Fig. 19 where values of u_* are depicted, which were derived from routine measurements.We conclude that terrain induced changes in friction velocity can amount to a factor 2 to 3. The Obukhov lenght may vary by an order of magnitude due to its cubic dependence on u_*.
Mixed-layer height development and, consequently, vertical diffusion is strongly L and u_* dependent (Tennekes, 1973), and through this dependence considerably terrain induced.

5. The dry deposition velocity.

A large fraction of released pollutants return to the earth's surface within a few days, by either dry or wet deposition.
The deposition velocity at an arbitrary height z can be related to a deposition velocity at a reference height of 1 m (cf. Eq. 2.12).
For the purpose of interregional transport modelling we have adopted some values for the deposition velocity of sulfurdioxide from literature (Table A.II). Though the difference between the values is hardly significant, so that the use of one overall deposition velocity would do as well, we prefer the use of these different values. In any case this way of modelling also offers the framework to insert more reliable values in the future. The results of the terrainclassification in combination with the data in Table A.II are presented in Fig. 19.

It should be noted here that besides the variation in V_g, the terrain induced variation in the aerodynamic resistance r(z,1), can be considerable. For example, in stable conditions (Eq. (2.13)) reads:

$$r(z,1) = \frac{0.74}{k\, u_*} \{\ln z + 5.4\, z/L\} \,. \qquad (A.4)$$

Typical values over relatively smooth terrain of u_* and L are 0.1 ms^{-1} and 20 m, so that the resistance of the layer 1-25 m amounts to $\sim$ 200 m^{-1} s, which inhibits strongly the deposition, even when V_g itself is high. In rougher areas u_* is usually larger (cf. Fig. 18) and r(z,1) diminishes accordingly, which suggests that - in stable conditions (> 50% of the time at moderate latitudes) - deposition of SO_2 is to a large fraction terrain induced.

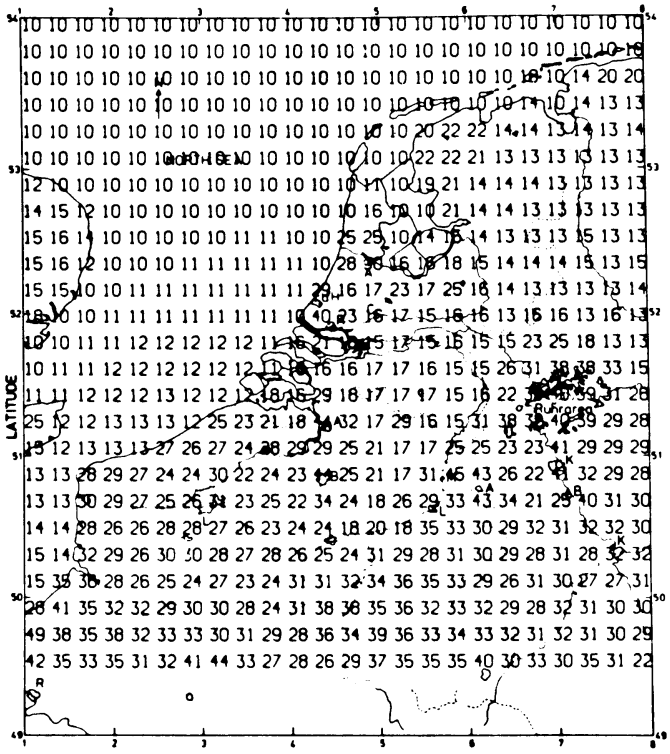

Fig. 19. The friction velocity u_* (cms^{-1}), 29 May,00 GMT. Note the relatively high values in the urbanised and forestal (southeast) areas. The values are representative for squares of 20 x 20 km^2. The correspondent 850 mbar windfield is fairly homogeneous and varies in from 3.5 to 6.6 m/s.

Table A.II. Deposition velocity for the combination of SO_2 and some terrain categories.

Terrain category	deposition velocity (cms^{-1})	reference
water surface	0.4	Garland, 1979
open field	0.8	Garland, 1979
open field with scattered trees and hedges	0.8	Garland, 1979
wood	0.6	Sehmel, 1980
buildings	2.0	Young, 1978 (in Sehmel, 1980) Van Dop et al., 1980a
roads/railways	0.1	Sehmel, 1980

According to tables A.I and A.II this means that SO_2 deposition will be strongly enhanced in forestal and urban areas. This underlines the potential importance of the inclusion of terrain features in atmospheric transport models.

Smith and Carson have undertaken an attempt to classify the terrain roughness of the UK. Though they followed a similar, but slightly different method their results compare reasonably well with ours (Van Dop, 1983). However, our method results, especially in rougher terrain, in higher values.

6. Correction of synoptic wind data for surface roughness.

The usual synoptic wind observations are done at a height of ~ 10 m. Though their locations are usually choosen with some care, they will be influenced by local terrain circumstances. In interpolation procedures, where these data are used (Van Dop et al., 1980b), it is desirable to remove any local influence before interpolation of the data. For that purpose all observed wind velocities are corrected for the small scale local roughness. The procedure is given by Wieringa (1976). After interpolation the inverse correction is applied to the resulting wind field in accordance with the large scale terrain roughness.

Though the corrections might seem a little superfluous in view of the large amount of uncertainties and inaccuracies involved in interregional modelling of air pollution transport, they surely improve the wind field interpolation in areas with large water surfaces, because of the large land-sea difference in surface roughness.

As an example we show in Fig. 20 the result of an interpolated wind field at 10 m height (29 May, 00.00 GMT). It is obvious that by applying the above procedure, the (observed) stronger wind field over the sea is not affected by the interpolation procedure, and that the relatively sharp gradient in the coastal zone is maintained.

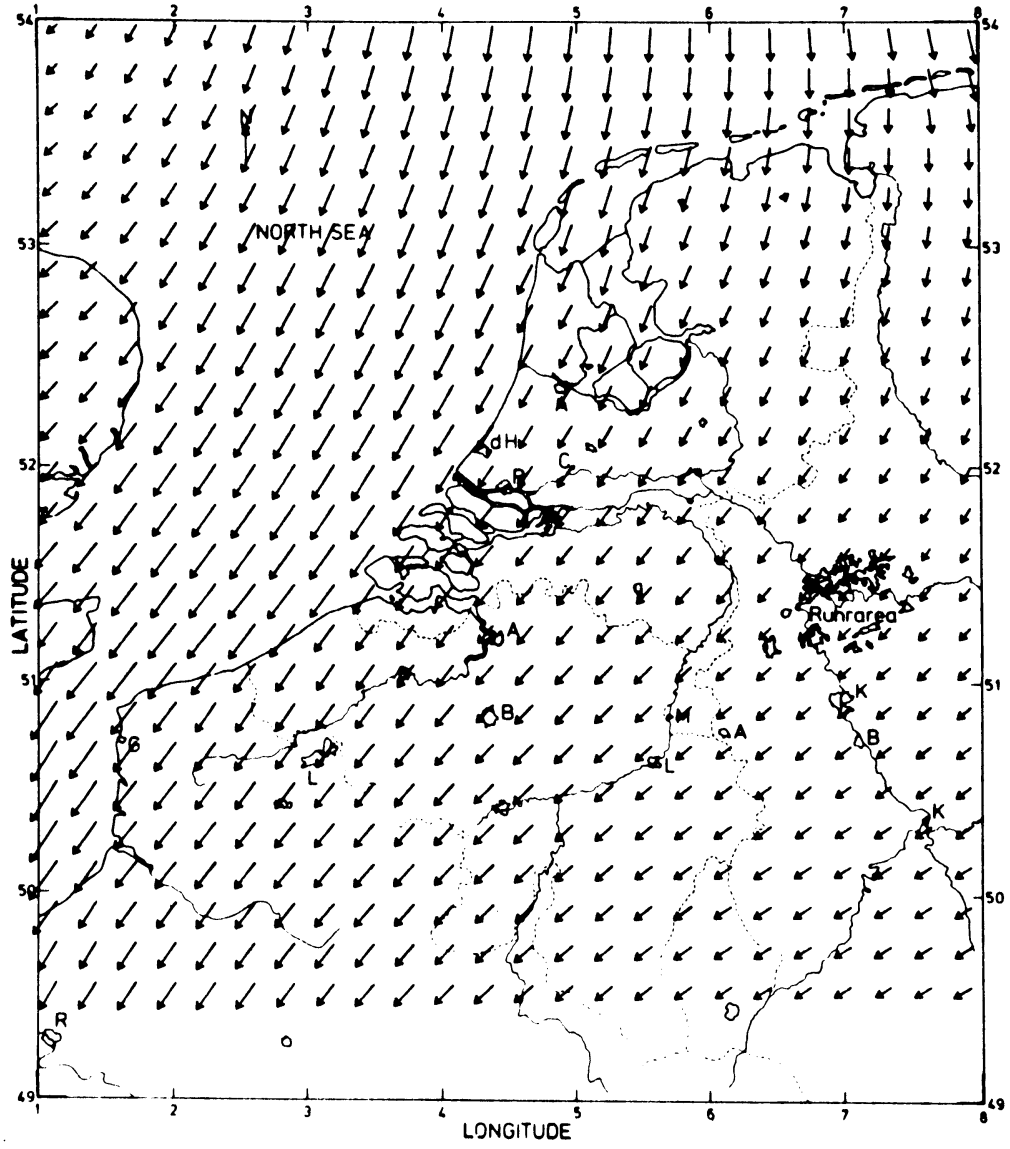

Fig. 20. Interpolated 10 m wind field (29 May, 00 GMT). Observe that the wind speed is markedly higher over sea, than over land.

APPENDIX B: A comparison of finite difference schemes, describing the two-dimensional advection equation.

In this appendix we compare some current numerical methods regarding accuracy and efficiency. The test problem is the commonly used advection of a cone in a rotating velocity field (e.g., Molenkamp 1968, Crowley 1968, Orszag, 1971).

1. The advection equation.

In a two dimensional rectangular coordinate system, the differential equation describing advection reads

$$\frac{\partial c}{\partial t} + u \frac{\partial c}{\partial x} + v \frac{\partial c}{\partial y} = 0 \qquad \text{(B.1)}$$

where c is the quantity advected, t the time, x and y the position coordinates and u and v the velocities in the x and y directions, respectively.
The integration domain is the square, $\{-1, 1; -1, 1\}$. At the inflow boundary we have the condition $c = 0$.

In the test the initial condition for the quantity c is a cone-shaped distribution with a base width of 0.5, centered at $\{-0.5, 0\}$.
The rotating velocity field is represented by $u = -\omega y$, $v = \omega x$, where ω is the angular velocity. The integration time is chosen equal to the rotation time. The conditions used are the same as the ones used in previous studies (for a detailed description see Orszag, 1971). Under certain conditions the velocity field of the atmosphere is approximately divergence free

$$\frac{\partial u}{\partial x} + \frac{\partial v}{\partial y} = 0.$$

However, the velocity field used in the test is even more constrained because not only

$$\frac{\partial u}{\partial x} + \frac{\partial v}{\partial y} = 0, \text{ but also}$$

$$\frac{\partial u}{\partial x} = \frac{\partial v}{\partial y} = 0.$$

Nevertheless we will use this particular field because of the availability of an exact solution.

2. Finite Difference Schemes.

One of the most simple schemes is the so called Euler explicit scheme, which is based on finite difference approximations of first and second order;

$$\frac{\partial c}{\partial t} = \frac{c^{n+1}-c^{n}}{\Delta t} + O(\Delta t), \quad \frac{\partial c}{\partial x} = \frac{c_{i+1}-c_{i-1}}{2\Delta x} + O(\Delta x^2) \ . \qquad (B.2)$$

A scheme is called explicit if the value of the quantity c at time (n+1) is computed explicitly from values of c at (a) previous time (s). The Euler explicit scheme reads

$$c_i^{n+1} = c_i^n - \tfrac{1}{2}\lambda c_{i-1}^n \ , \qquad (B.3)$$

with Courant number $\lambda = u\Delta t/\Delta x$.

There are two ways to improve the accuracy of this scheme. One way is to choose higher order approximations for either of the derivatives, the other way is to start from a Taylor series in t. The time derivatives are then substituted with Eq. (B.1) by expressions containing only space derivative terms (Richtmeyer and Morton (1967). Schemes designed this way are called "characteristic interpolation" or "quasi-Lagrangian" schemes. An example is the second order Lax Wendroff scheme. This scheme reads

$$c_i^{n+1} = c_i^n - \tfrac{1}{2}\lambda(c_{i+1}^n - c_{i-1}^n) + \tfrac{1}{2}\lambda^2(c_{i+1}^n - 2c_i^n + c_{i-1}^n) \ . \qquad (B.4)$$

A straightforward extension of the Euler explicit scheme is a second order centered difference approximation for the time derivative to be combined with second (leap-frog method), fourth or even sixth order centered difference approximations for the space derivatives. A fourth order approximation for the time derivative -trapezium rule or Runge Kutta 4 method- in combination with the fourth order centered difference approximation for the space derivatives has been used for the solution of the shallow water equations (Praagman, 1979, Praagman and Segal, 1974).

Two efficient higher order approximations for the space derivatives have been introduced. The first, the compact differencing technique, has been used in combination with both explicit and implicit first order approximations for the time derivative (Adam, 1977). The introduction of fast Fourier transform (FFT) algoritms promoted the use of the pseudo spectral method. This method has excellent resolution and accuracy properties (Fox and Orszag, 1973).

Some "characteristic interpolation" schemes are truly extended to two dimensional advection, while others are a result of solving the one dimensional advection equation in alternating directions. A fourth order extension of the two dimensional Lax Wendroff scheme was proposed by Gadd (1979). Most attention, however, was paid to one dimensional schemes (see e.g., Wesseling 1972). The fourth order schemes (e.g., Crowley, 1967) show considerable improvement over the Lax Wendroff scheme.

The introduction of compact differencing and fast Fourier transform techniques led with respect to the "characteristic interpolation" schemes also to very accurate schemes (Forester, 1977, Gazdag, 1973). The computation costs, however, increased sharply. A scheme of lower order using the compact differencing technique (Purnell 1976) appeared to be more efficient.
From the variety of schemes discussed above a few have been selected to make a comparison. The schemes chosen are the two step Lax Wendroff scheme (to be referred to as LW), the fourth order extension of the scheme LW (G), the compact differencing upstream interpolation scheme (P), the fourth order in time and space scheme (RK4) and the pseudospectral method (FFT).

3. Numerical Tests.

The effiency of a method may be expressed in terms of accuracy and computation costs. The results of the test are summarized in Table B.1.
The process time dependents on the number of timesteps (N) and the mesh size (GRID) chosen for the schemes. The mesh size was 32 x 32 for all schemes, but the pseudospectral method - considered the good resolution (Orszag 1971) and the expense of the fast Fourier transform - may be compared with these methods using a 16 x 16 grid only. The cone width is four gridpoints on the 32 x 32 mesh and two on the 16 x 16 mesh. None of the schemes have been filtered. All computations have been carried out on a Burroughs 6700 computer. The programmes were not optimized.

Table B.1. A comparison of five numerical advection schemes. The gridsize (GRID) denotes the number of gridpoints; N is the number of timesteps; MAX denotes the centre cone value after one revolution (initially 100); LAG denotes the difference in position (degrees) between the exact and the numerical solution; the processtime (CPU) is indicated in the last column.

method	reference	GRID	N	MAX	LAG	CPU (s)
LW	Richtmeyer and Morton	32x32	200	49	27	109
G	Gadd	32x32	200	80	-4	213
P	Purnell	32x32	100	82	0	173
RK4	Praagman	32x32	100	81	5	296
FFT	Fox Orszag	16x16	200	96	1	108

4. Conclusions.

The properties of the schemes become clear when we see the images of the distribution of the quantity c as a series in time. During the first part of the rotation most schemes round off the sharp discontinuities of the cone, making the cone more bell-shaped. In the last part this type of diffusion of the cone is small.

The schemes G, P and RK4 reduce the maximum cone value to ~ 80% of the original value. The time lag and the computation time considered, method P is the best. However, method P makes use of the property of the velocity field

$$\frac{\partial u}{\partial x} = \frac{\partial v}{\partial y} = 0 \ ,$$

which makes it doubtful whether the scheme will perform as well with more general velocity fields.
The pseudo spectral method behaves also better than we may aspect under more general circumstances, because it requires that c is periodic. This results in the reappearance of the quantity c on the one boundary when being advected out over the opposite boundary. Two remedies to avoid this have been proposed. One is to introduce an artificial drain term at the grid boundaries of the form $-c(x,y,t)/\tau(x,y)$ in the advection equation. The decay constant $\tau(x,y)$ can be chosen such that it assumes realistic values, appropriate to the physical

situation (Christensen, Prahm 1976). The second proposal is to decompose the distribution of quantity c in a periodic and a polynomial part. The treatment of the advection of the concentration distribution which is represented by the (third degree) polynomial is straight forward. By a special choice of the coefficients of the polynomial it is achieved that the complementary periodic function and its derivative have zero values at the boundaries. In this way it is possible to avoid the discontinuity at the boundary. Also transport over the boundary and consequently the impact at the oppsite boundary was minimized in this way (Wengle and Seinfeld, 1978).
The latter method was applied in the transport model.

The pseudo spectral method is more efficient than any other of the tested methods with only one fourth of the number of gridpoints in the model. A drawback in practical problems, however, is the requirement of periodicity.

The reduction of the number of gridpoints, however, is certainly attractive for three dimensional models. because the number of gridpoints and, consequently, the data requirements and the number of computations in the vertical direction are reduced by a factor of four.

APPENDIX C: The wind and turbulence field.

1. Time interpolation.

The observed meteorological data should be converted to regular grids and time intervals. The time step in our case is one hour, though not all observations are hourly available. It frequently happens that synoptic reports are released every three hours or with varying frequency, depending on the time of the day. Also instrument or transmission line failure may be the cause of irregular time series of observations. We have chosen for simple linear interpolation to complete time series where sometimes data are missing.

2. Spatial interpolation (horizontal)

Now we have at each time step the same set of data, which will be used for the spatial interpolation. First all data are interpolated in horizontal planes.

2.1. 10 m wind velocity

Approximately 60 synoptic stations in the region have been selected (cf. Fig. 9). The wind observations are interpolated by means of the optimum interpolation method (Cats, 1980), the basic interpolation formula is given by e.g.,

$$U_a = \langle U_a \rangle + \sum_{i=1}^{n} W_{ia} \, (U_i - \langle U_i \rangle) \, , \qquad (C.1)$$

where U_i is the observed West-East component of the wind velocity at the i-th synoptic station (with a total number of n). The index a marks the interpolation or gridpoint. The brackets indicate time averaged values. The weighting function is given by:

$$W_{ia} = \sum_{j=1}^{n} (C_{ij})^{-1} \, C_{ja} \, , \qquad (C.2)$$

where C_{ij} is the covariance of the observations of U at the stations i and j:

$$C_j = \langle (U_i - \langle U_i \rangle) \, (U_j - \langle U_j \rangle) \rangle \, . \qquad (C.3)$$

The covariance and the average are expressed in simple functions of the horizontal spatial coordinates by means of least square fitting of the data.

The interpolation method has the advantage that gradients of U can be easily obtained by means of differentiation of (C.1). A drawback of the method is that application requires the knowledge of statistical properties of the observations used.
For the surface wind observations a correction has been applied to remove the influence of local terrain roughness before the interpolation is carried out (see Appendix A). The correction is given by:

$$U_c = U_{10} \cdot \frac{\ln(10/0.03)\ \ln(60/z_o)}{\ln(60/0.03)\ (\ln 10/z_o)} , \qquad (C.4)$$

(Wieringa, 1976). The local roughness length is denoted by z_o. The correction is essentially an upward extrapolation of the 10 m wind to 60 m - assuming a neutral surface layer (local roughness z_o) - and a subsequent extrapolation downward to 10 m, but now using a (standard) roughness of 0.03 m. The inverse operation is applied to the interpolated field.
In the interpolation procedure an internal check compares the interpolated values at the synoptic stations with the observed ones. When at a particular station the difference between the two values is larger than a prescribed value, the observation at that station is rejected and the interpolation is repeated, until optimum agreement is obtained between observed and interpolated data.
Interpolated wind data have been compared with observations at Cabauw. The results are given in Fig. 21.

2.2. Surface pressure

The same procedure as in section 2.1. is followed to obtain an interpolated pressure field. The geostrophic wind components,

$$(U_g, V_g)^o = -\frac{1}{\rho f}\left(\frac{\partial P}{\partial y}, -\frac{\partial P}{\partial x}\right) , \qquad (C.5)$$

are obtained by differentiation of the interpolation formula (c.f. equation (C.1)). An example is given in Fig. 22, where the interpolated data are compared with the 850 mbar radiosonde analysis of the windfield.

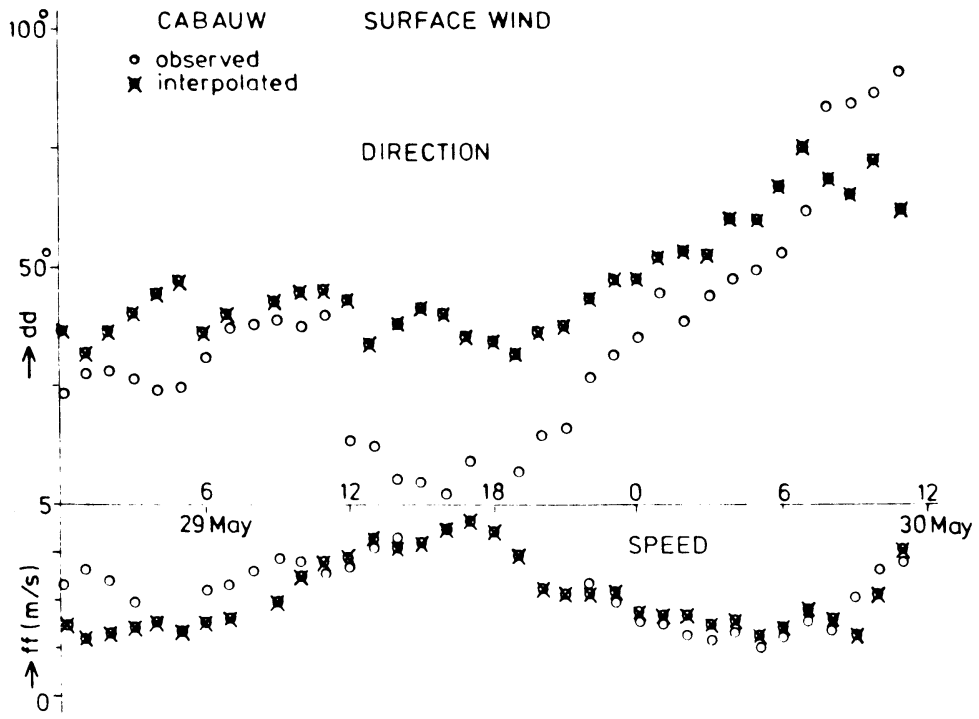

Fig. 21. Observed and interpolated 10 m wind at Cabauw (10 m height).

2.3. Surface temperature

Again the optimum interpolation method is used. The temperature field over land is determined from observations over land only (the higher situated stations are excluded). The air temperature over sea is derived from lightvessel (or platform) observations. As a consequence the interpolation yields less accurate temperatures in coastal and elevated areas. This is illustrated in Figure 23.

2.4. 850 mbar wind

Radiosonde data are interpolated according to:

$$(U_g, V_g)^1 = \sum_{i=1}^{m} (U_i, V_i)^{850} \cdot W_i / \sum_{i=1}^{m} W_i \,, \qquad \text{(C.6)}$$

where W_i is the weighting function,

$$W_i = (r_i^2 + a^2)^{-1} \,.$$

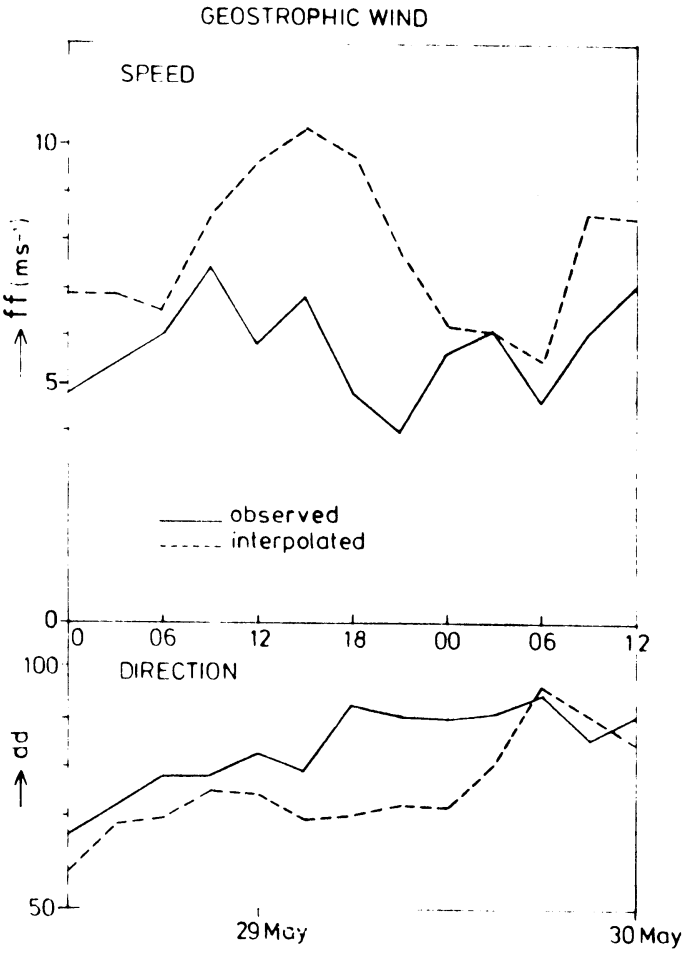

Fig. 22. Interpolated groundlevel geostrophic wind speed and direction at Cabauw. The observed 850 mbar radiosonde analysis is depicted by the solid line. The sometimes large differences may be ascribed to baroclinic effects.

The distance between the observation and interpolation point is given by r_i and the "radius of influence" of the data is denoted by a. It is of the order of a few hundred km (Cats, 1980). In (C.6), m denotes the number of observations. In or near the region concerned are seven stations which report two to four times daily. Again an example of the interpolated data is given in Fig. 23 and compared with observations in Cabauw.

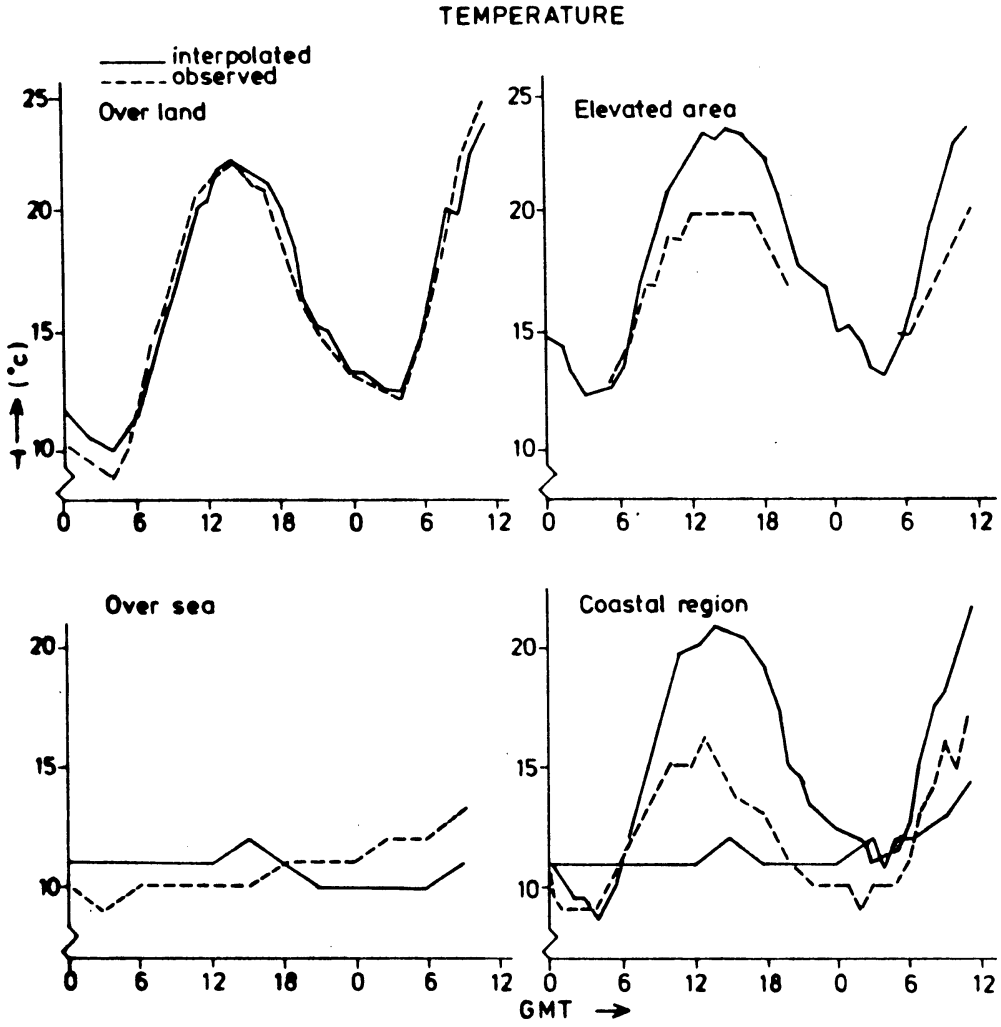

Fig. 23. Observed and interpolated temperatures (observation height ~ 1.5 m) at 4 sites.

2.5. Wind measurements at towers and masts

These data are very useful because they are done at heights (50-300 m) where the wind velocity may be strongly varying (e.g., low level jet). They are incorporated in the wind field in a way which will be described below in section 4.1.

2.6. Cloud cover

The cloud cover plays an important role in the determination of the atmospheric stability, and should therefore be included in the formulation. The interpolation of cloud cover data should, however, be done with care: clouds can be present very intermittently both in space and time. Also cloud patterns possess their own spatial characteristics (e.g. frontal clouds, convective clouds), which may be difficult to average. We therefore did not average cloud cover data but assigned to each gridpoint the cloud cover which was reported by the nearest synoptic station.

2.7. Lapse rate

Inversion rise models (Driedonks, 1981) require as input the temperature lapse rate of the (stable) layer above the capping inversion. The lapse rate is obtained from the 00 GMT radiosonde (which is approximately midnight in Europe). Conversion to potential temperature (Θ) is done simply by:

$$\partial\Theta/\partial z = \partial T/\partial z + \Gamma \ , \qquad (C.7)$$

where Γ ($= g/C_p$) is the dry-adiabatic lapse rate. When negative values of $\partial\Theta/\partial z$ are encountered $\partial\Theta/\partial z$ is set to zero. When data are missing a representative stable lapse rate equal to $5\ 10^{-3}$ Km^{-1} is assumed. Interpolation is done by a $1/r^2$ method.

3. Derived meteorological parameters

There exists a wealth of data on the quasi-stationnary horizontally-homogeneous boundary layer. These will be used to characterise the vertical wind and turbulence structure, though we realise that this is not a correct procedure during transient periods (day-night transition and v.v.) and in areas where the surface properties strongly change (land-sea transition). The parameters which are relevant for the atmospheric boundary layer are the friction velocity, u_*, the roughness length z_o, the Obukhov length, L and the boundary-layer height, z_i. Before we discuss the wind and turbulence structure we will summarise how these parameters were determined.

3.1 L and u_*

They can be determined iteratively from:

$$U = (u_*/k)\,\{\ln(z/z_o) - \psi_1(z/L)\}$$

and

$$L = -T\,u_*^3/(kg\,\overline{\theta w}_o)\ , \qquad (C.8)$$

when for U the 10 m wind speed is taken, $\overline{\theta w}_o$ is derived from the sensible heat flux Q ($= \rho C_p\,\overline{\theta w}_o$) . The average absolute temperature of the boundary layer is denoted by T and k is Von Karman's constant (here equal to 0.35).
The stability dependent function ψ_1 is given by:

$$L < 0:\ \psi_1 = 2\ln\left(\frac{1+x}{2}\right) + \ln\left(\frac{1+x^2}{2}\right) - 2\,\mathrm{arctg}(x) + \pi/2,$$

$$x = \left(1 - \frac{15z}{L}\right)^{\frac{1}{4}} \qquad (C.9)$$

$$L > 0:\ \psi_1 = -4.7\ z/L\ .$$

The surface heat flux Q is determined in the following way:

- over land, daytime (solar elevation > 15^o)

In this case Q is given by:

$$Q = \frac{(1-\alpha)S + \gamma}{S + \gamma}\,(Q^* - G) - \beta\ , \qquad (C.10)$$

(De Bruin and Holtslag, 1981). In (10) α and β depend on the terrain type (see Appendix A). The empirical temperature dependent functions γ and S are given by:

$$\gamma = 0.646 + 6.10^{-4}\,(T - 273.1)$$

and

$$S = 4.10^3\,\varepsilon(T)/T - 35.8)^2\ , \qquad (C.11)$$

$$\varepsilon(T) = 10^{\left\{\frac{7.5(T-273.1)}{T-35.8} + 0.786\right\}}\ .$$

The soil heat flux is taken equal to 0.1 Q^*, where Q^* denotes the net

radiation. It is calculated from:

$$Q^* = 1258(1-\alpha_1)\ \sin(z)(a+b\ \sin(z))(1-0.7\ N^2) + 60\ N$$
$$+ 5.31\ 10^{-13}\ T^6 - 5.67\ 10^{-8}\ T^4\ . \qquad (C.12)$$

The albedo (α_1), and the constants a and b have the values 0.25, 0.48 and 0.29 respectively. The cloud cover fraction is denoted by N. In (C.12) z denotes the solar elevation.

- over land, nighttime (solar elevation < 15°)

When $z < 0$ we use:

$$Q^* = -\frac{90}{1 + 4/U^2}\ (1 - 0.9\ N^2)\ , \qquad (C.13)$$

where U is the 10 m windspeed (Holtslag and Van Ulden, 1982). (When $U < 2\ ms^{-1}$ then the nominator in (C.13) is put equal to 2.)

For solar elevations between 0° and 15° a linear combination of the expressions (C.12) and (C.13) is applied that warrants a smooth day-night transition and vice versa.

When Q^* turns out to be negative (C.10) no longer applies. Instead we use:

$$Q = 0.4\ Q^*\ . \qquad (C.14)$$

(Eq.(C.14) is also applied when during daytime negative Q_* values are evaluated.)

An alternative method in stable conditions ($L > 0$) is indicated by Venkatram (1980). Based on observations he puts Q proportional to u_*, where the constant of proportionality is $-93\ Wm^{-3}s$:

$$Q = -93\ u_*\ . \qquad (C.15)$$

However, as shown in Fig. 24 the differences are small.

- Over water.

We now encounter a situation where the latent heat flux largely exceeds the (small) sensible heat flux. Because the stability of the atmosphere is determined by its density gradient, not only the temperature influence on the density but

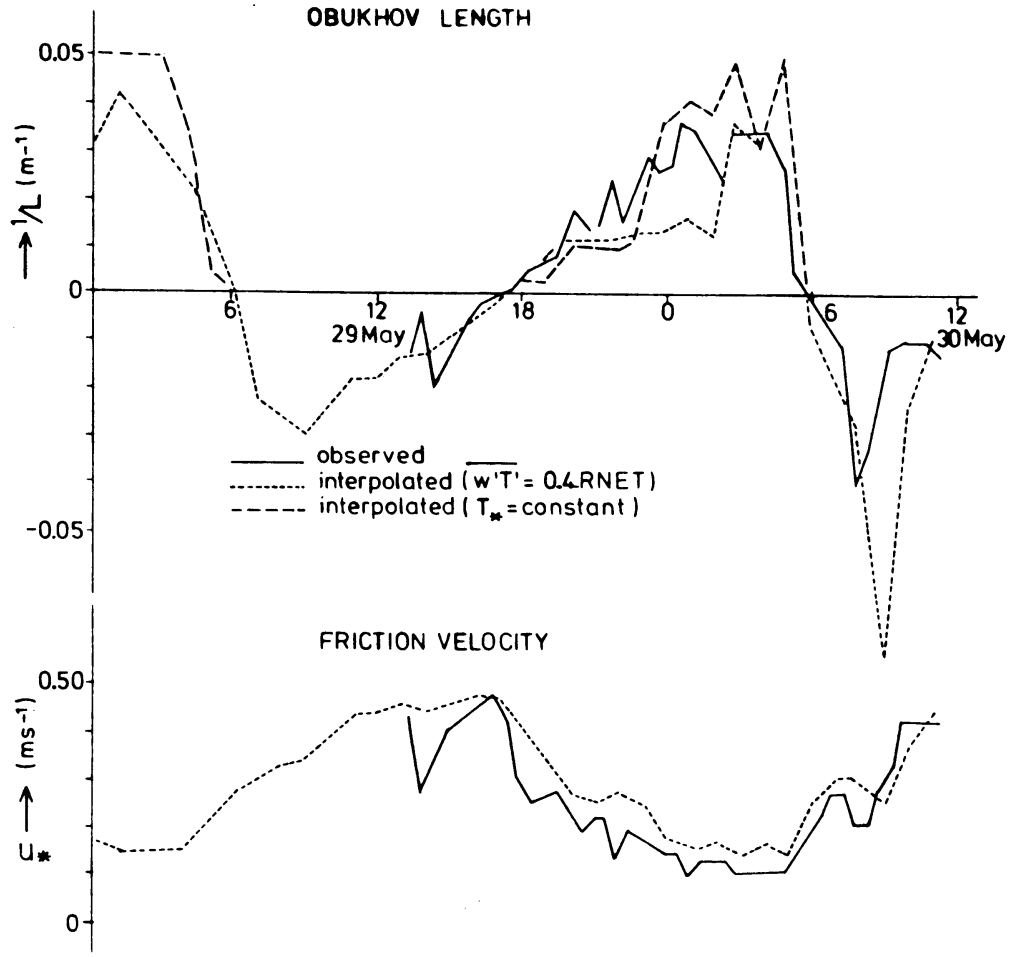

Fig. 24. Interpolated turbulence parameters (L and u_*) compared with observations in Cabauw. The observed L and u_* were obtained from direct measurements of the turbulent fluxes of heat and momentum. The value of L according to Eq. (C.15) is also depicted (T_* = constant).

also the water vapour content should be taken into account. This can conveniently be done by the introduction of the virtual potential temperature T_v. The Obukhov length may than be written as:

$$L = -T\, u_*^3/[kg\, (\overline{\theta w}_o + 0.61\, T\overline{qw})] \,, \qquad (C.16)$$

where $\overline{\theta w}_o = Q/\rho C_p$ as before, and $\overline{wq}$ denotes the humidity flux (q is the specific humidity). Over sea they are determined from the following expressions:

$$\overline{\theta w}_o = C_h (U-U_s)(T_w - T)$$

and (C.17)

$$\overline{qw} = C_q(U - U_s)(q_w - q) .$$

The surface wind velocity U_s, is taken zero, the water surface temperature is denoted by T_w. When the dew-point temperature, T_d - a more familiar quantity in synoptic meteorology is known, then the specific humidity can be derived from

$$q = 3.8\ 10^{-3}\ 10^{\left\{\frac{7.5\ T_d}{237.3 + T_d}\right\}} . \qquad (C.18)$$

In (C.16) u_* is obtained from

$$u_* = C_d^{\frac{1}{2}} (U-U_s) . \qquad (C.19)$$

The "drag coefficients" $C_{d,h,q}$ are all taken equal to $1.5\ 10^{-3}$.
When values of u_* smaller than 0.1 ms^{-1} result from the calculations, u_* is set to 0.1 ms^{-1}. Also the magnitude of L is limited to a minimum value of 20.

3.2. The inversion height z_i.

Both the nocturnal inversion height and the day-time mixed layer height will be denoted by z_i. A steady state expression is used for the determination of the nocturnal boundary-layer height (Nieuwstadt, 1981a, b). It is based on the similarity expression:

$$z_i = 0.4(u_* L/f)^{\frac{1}{2}} , \qquad (C.20)$$

(Brost and Wyngaard, 1978). It is modified such that in neutral conditions the expression for the neutral boundary-layer height results. Hence,

$$z_i = \frac{0.3\ u_*/f}{1 + 1.9\ z_i/L} . \qquad (C.21)$$

After solving z_i from (21) we get:

$$z_i = 0.26\ L\{(1 + 2.04\ 10^4\ u_*/L)^{\frac{1}{2}} - 1\} . \qquad (C.22)$$

This expression is supported by some observational evidence (Fig. 25). Though through the dependence on $u_*(t)$ and $L(t)$, the z_i-values vary from hour to hour, we will neglect this variation in stable conditions and use a time-averaged nocturnal boundary-layer height. Its spatial variation will, however, be maintained. It should be noted that (C.20) may also be used during daytime*, in stable, predominantly overcast conditions (cloud cover N > 5).

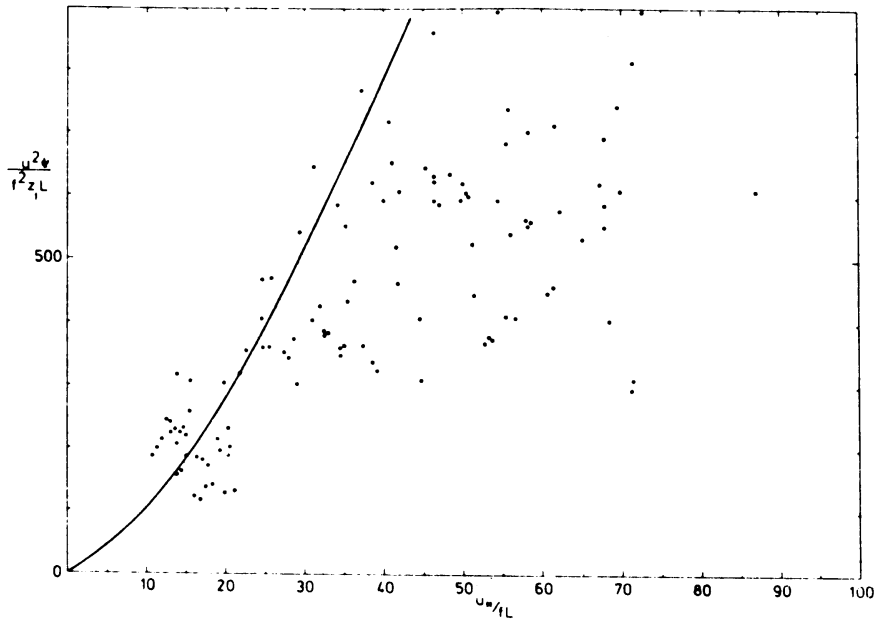

Fig. 25. A comparison between Eq. (C.22) (solid line) and observations of the nocturnal boundary-layer height at Cabauw.
(By courtesy of Dr. F.T.M. Nieuwstadt, 1980).

Stable situations during sunny conditions are supposed not to occur or, if reported, ascribed to observational error.
In unstable conditions ($L < 0$), it is assumed that a mixed layer exists, which height is non-descending. Buoyancy as well as mechanical forces will cause the inversion rise (Tennekes, 1973).
We resume here the equations:

* Daytime is defined as the period between one hour after sunrise and one hour before sunset.

$$\partial\Theta/\partial t = (\overline{\theta w}_o - \overline{\theta w}_i)/z_i \quad , \tag{a}$$

$$\Delta\ \partial z_i/\partial t = -\overline{\theta w}_i \quad , \tag{b}$$

$$\partial\Delta/\partial t = \gamma\ \partial z_i/\partial t - \partial\Theta/\partial t \quad , \tag{c}$$

$$-\overline{\theta w}_i = C_1\ \overline{\theta w}_o - C_2(T/g)\ u_*^3/z_i \quad , \tag{d}$$

(C.23)

where C_1 and C_2 are constants (0.2 and 2.5 respectively), γ denotes the lapse rate of the layer beyond the inversion, Θ the mixed-layer potential temperature, and Δ the inversion strength. The heat flux at the surface and at

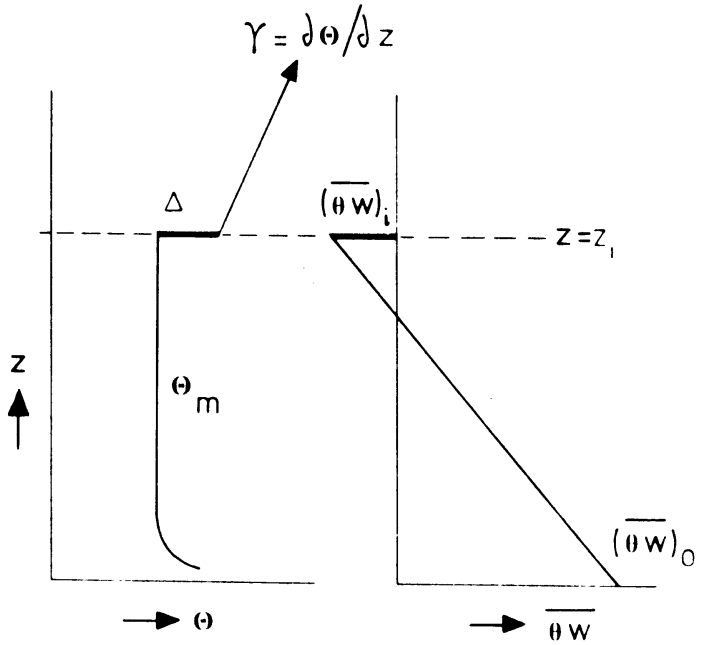

Fig. 26. Schematic representation of the thermal convective boundary layer structure. Δ denotes the inversion strength0 The heat fluxes at ground level and inversion height are respectively $\overline{\theta w}_o$ and $\overline{\theta w}_i$.
(By courtesy of Dr. A.G.M. Driedonks).

the inversion height are denoted by $\overline{\theta w}_o$ and $\overline{\theta w}_i$ respectively. (Most symbols are also explained in Fig. 26).

Once the initial conditions are given the set equation (C.23) can be solved

with standard numerical methods, provided that $\overline{\theta w}_o$ and γ are known functions of time.

We will use a somewhat simplified method where (hourly) stepwise increments in the boundary-layer height are calculated analytically.

We consider the two cases:

a. $C_1 \overline{\theta w}_o >> C_2(T/g)u_*^3/z_i$.

This condition is equivalent with $h/|L| >> k\, C_2/C_1$, by virtue of the definition of L (eq. (C.8)). This condition is often satisfied in a daytime boundary layer with not too strong winds (Lamb, 1982).

We thus neglect the second term in (C.23d) and solve the set (C.23). A solution for Δ is:

$$\Delta = \frac{C_1}{1 + 2C_1} \gamma\, z_i + O(z_i^{-6}) \ , \qquad \text{(C.24a)}$$

where O(..) means of the order of.

The last term in (C.24) will be neglected. Then an analytical expression for z_i's derivative is obtained:

$$\partial z_i/\partial t = \left(\frac{1 + 2C_1}{\gamma}\right) \cdot \frac{\overline{\theta w}_o}{z_i} \ . \qquad \text{(C.24b)}$$

b: $C_1 \overline{\theta w}_o << C_2(T/g)u_*^3/z_i$, or $0 < h/|L| << k\, C_2/C_1$. We have here a situation where the mixed-layer growth is dominated by mechanical turbulence. The solution of (C.23) is obtained by neglecting the first term at the right hand side of Eq. (C.23d):

$$\Delta = \tfrac{1}{2} \gamma\, z_i \ , \qquad \text{(C.25a)}$$

$$\partial z_i/\partial t = 2C_2/\gamma\ (T/g)u_*^3/z_i^2 \ , \qquad \text{(C.25b)}$$

We assume now that the general solution smoothly changes from (C.25) to (C.26) when $h/|L|$ varies from very large to small values. We therefore propose as an approximate solution to (C.23) a linear combination of (C.24b) and (C.25b). The coefficients are chosen proportional to the magnitude of $h/|L|$. A combination with the proper asymptotic behaviour is:

$$\partial z_i/\partial t = \frac{\overline{\theta w}_o}{\gamma\, z_i\left(1 - \left(\frac{k\, C_2}{C_1}\right)\frac{L}{z_i}\right)} \left[1 + 2C_1 + 2k^2C_2^2/C_1\ (L/z_i)^2\right] . \quad (C.26)$$

We obtain the inversion height at t + Δt from its previous value according to:

$$z_i(t + \Delta t) = z_i(t) + \Delta t\ \partial z_i/\partial t\ , \quad (C.27)$$

where the timestep Δt is equal to 1 hr.
The set equations (C.26, C.17) is compared with the "exact solution" of (C.23) and the agreement was satisfactory (Driedonks, 1980)*.
Running along with (26) is the equation for rate of change of the boundary layer temperature,

$$\partial\Theta/\partial t = \frac{\overline{\theta w}_o}{z_i} \left[1 + C_1 - k\, C_2\ L/z_i\right] , \quad (C.28)$$

which can be used to calculate the daily maximum temperature. For that purpose the boundary layer temperature is converted to the temperature at synoptic observation height (~ 1.50 m) by means of the relations:

$$\Theta - \Theta_o = 0.74\, \frac{\overline{\theta w}_o}{k\, u_*} \left\{\ln z/z_o - \psi_2\ (z/L)\right\} , \quad (C.29)$$

where ψ_2 is given by (2.13a). We have assumed that the mixed layer temperature is attained at a height of approximately 2.5 ‖L‖ . The calculated temperatures can be compared with the observed ones, and may serve as a consistency check for the applied method. An example is given in Fig. 27.

It should be noted that the methods used in this section are based on the dynamics of the atmospheric boundary layer in horizontally homogeneous conditions. As a consequence large errors may occur in the boundary-layer height determination in the coastal zone for example.

* private communication.

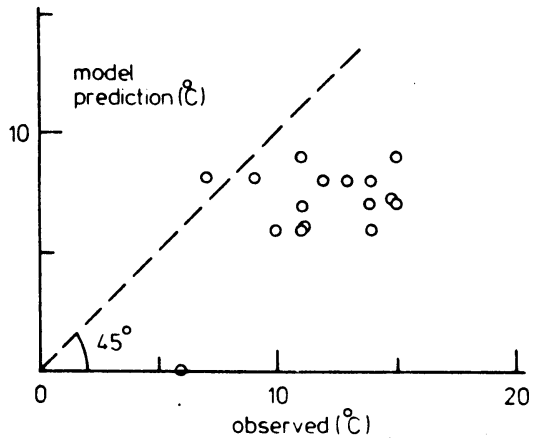

Fig. 27. Observed and predicted increase in ground level temperature during 29 May 1978. The observed values are the difference between minimum and maximum temperature. The model prediction is based on Eqs. (C.28, C.29).

4. Vertical Interpolation

4.1. The wind profile

With the data in the previous sections we are able to construct wind profiles at any desired place within the region.

The basis components of the wind profile are:

- the surface-layer wind profile

  From Fig. 28, where the atmospheric boundary layer is roughly sketched, we observe that the surface layer extends to $\sim 0.1\ z_i$. In steady and homogeneous conditions the profile is given by the empirical relation*

$$U_s(x,y;z) = U_c \frac{\ln(z/z_o)-\psi_1(z/L)}{\ln(10/z_o)-\psi_1(10/L)}\ , \qquad (C.30)$$

  where ψ_1 is given by Eq.(C.9).

* For simplicity we present the x-component, U_s, only, the expressions for the y-component being similar.

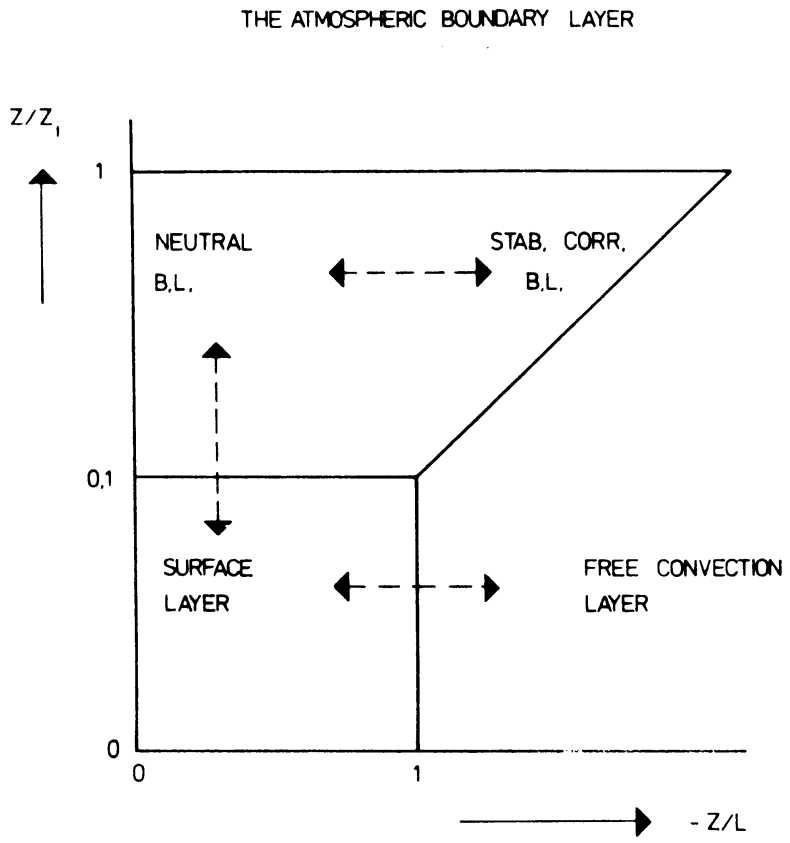

Fig. 28. Sketch of the atmospheric boundary layer according to stability (z/L) and height (z/z_i).

In (C.30), U_s is chosen such that it passes through the (interpolated and local roughness length corrected) wind speed at 10 m, U_c (cf. Eq. (C.4)). The dependence on the horizontal coordinates is through U_c, L and $z_o(x,y)$.

- The geostrophic wind profile.

The spatial derivatives of the surface pressure field provide the surface level geostrophic wind U_{g0}. The 850 mbar wind velocity is linearly interpolated, and provides the 850 mbar geostrophic wind, U_{g1}. The geostrophic wind profile is obtained by linear interpolation of U_{g0} and U_{g1} according to

$$U_g(x,y;z) = \frac{(z_1-z)U_{go} + (z-z_s)U_{g1}}{z_1 - z_s}, \qquad (C.31)$$

where z_1 and z_s are the levels where U_{g0} and U_{g1} are determined (respectively at 1.5 m and ~ 1500 m).

- The mast and tower data.
  Wind velocity measurements along masts are interpolated by means of a third degree polynomial,

$$U_m(X_m,Y_m;z) = a\ z^3 + b\ z^2 + c\ z\ . \qquad (C.32)$$

  The constants a, b and c are determined by the constraints that (i) $U_m(z) = U_g(z)$ and $\partial U_m/\partial z = \partial U_g/\partial z$ at a fixed level (z = 500 m), and (ii) by a least square fit of the observations along the mast. Finally the mastprofiles are interpolated horizontally, yielding the velocity field $U_m(x,y,z)$.

The three profiles, U_s, U_g and U_m are now integrated into one final profile by taking linear combinations,

$$U = \alpha_a\ U_s + \alpha_g\ U_g + \alpha_m\ U_m\ . \qquad (C.33)$$

The weighting functions α_s, α_g and α_m are determined according to the scheme in Fig. 29. In the intermediate regions, where a "mixture" of two profiles is used the weighting functions are chosen such that a smooth transition is assured to the neighbouring regions.
The thus obtained horizontal wind field will in general not be divergence free, i.e.

$$\partial U/\partial x + \partial V/\partial y \neq 0\ . \qquad (C.34)$$

The imbalance is caused on the one hand by measuring errors and model assumptions, and on the other by the presence of vertical movement, which according to the full non-divergence equation for an incompressible fluid is given by:

$$W(z) = -\int_0^z \left(\frac{\partial U}{\partial x} + \frac{\partial V}{\partial y}\right) dz'\ . \qquad (C.35)$$

It is expected that over more or less flat terrain the (hourly) mean vertical motion will be small, and presumably not exceed the involved inaccuracies. Therefore, the divergence which the derived U, V field might possess is removed by a procedure given by Endlich (1967). The use of divergence-free

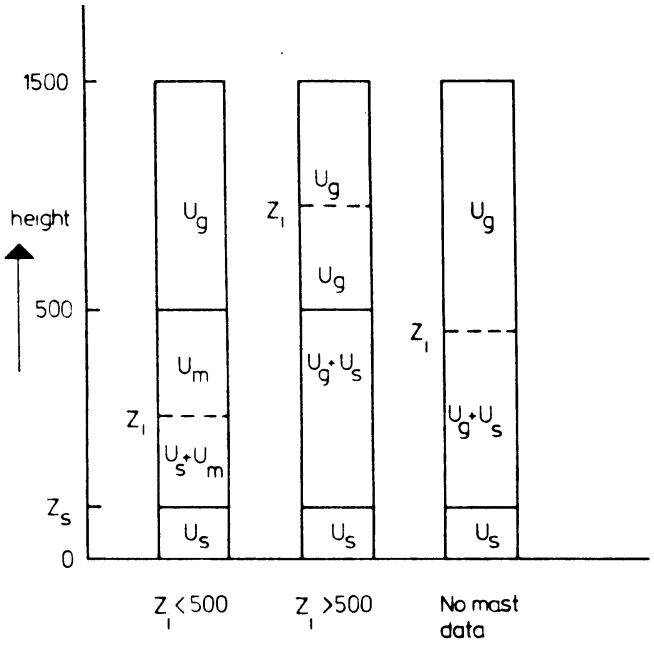

Fig. 29. Review of the use and assembling of winddata in the atmospheric boundary layer, at various heights. The construction of this picture is largely based on fig. 28.

fields avoids numerical errors which arise when in locally strong convergent areas an accumulation of pollutant concentrations occurs. Then steep gradients may result, which affect the numerical accuracy unnecessarily.
An example of what kinds of wind fields are obtained from this routine is given in Fig. 30 and Fig. 31.

4.2. The eddy diffusivity

It is assumed that the turbulent transport of material equals that of heat, though the latter is not really a passive contaminant. We adopt an expression given by Brost and Wyngaard (1978),

$$K_z = \frac{k\, z\, u_*(1 - z/z_i)^{1.5}}{\phi(z/L)}, \quad z < z_i \qquad \text{(C.36)}$$

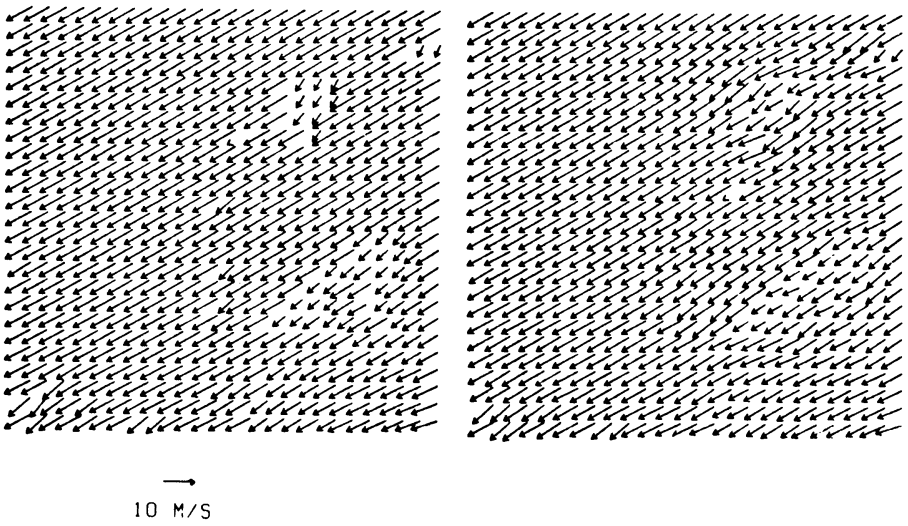

Fig. 30. An interpolated wind field at 200 m height; (a) original and (b) divergence free (29 May 1978, 00 GMT).

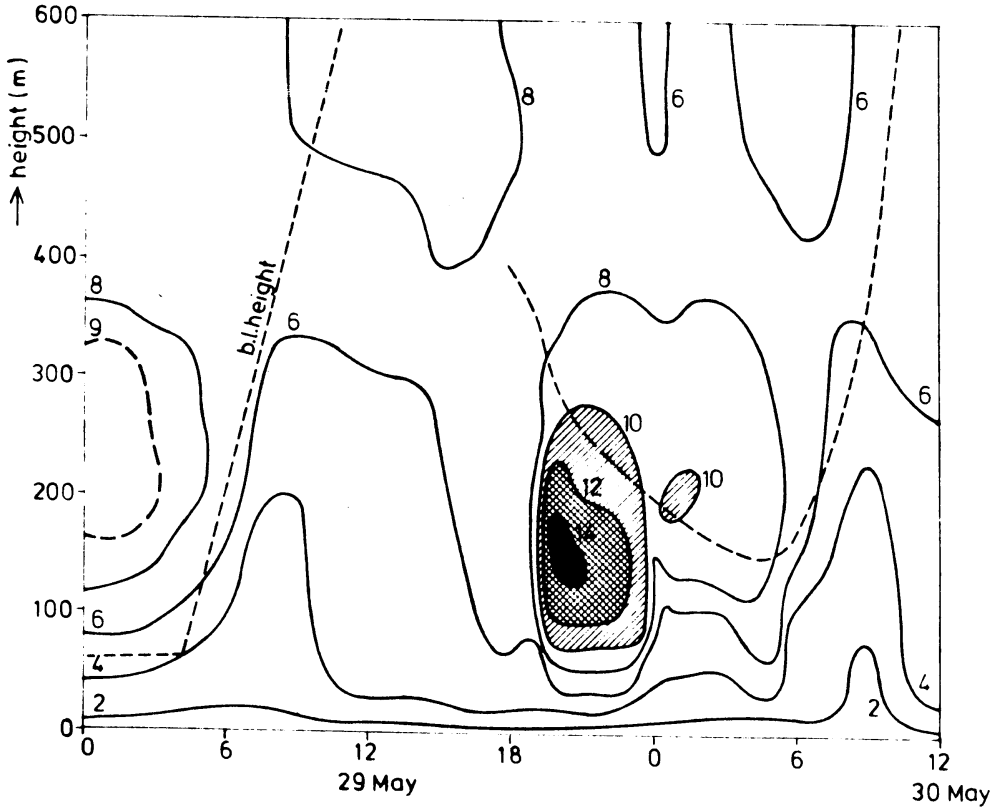

Fig. 31. Time height cross section of the interpolated wind speed at Cabauw. Isopleths are drawn every 2 ms^{-1}. On 29 May also the 9 ms^{-1} isopleth was drawn in order to indicate the low level jet more clearly.

where for $L > 0$,

$$\phi(z/L) = 0.74 + 4.7\ z/L\ ,$$

and for $L < 0$,

$$\phi(z/L) = 0.74(1 - 9\ z/L)^{-\frac{1}{2}}\ .$$

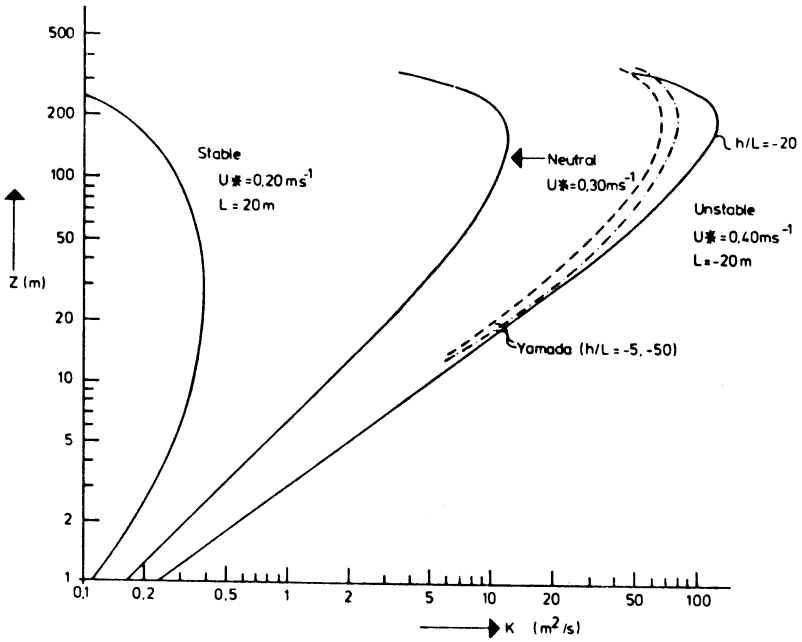

Fig. 32. Profiles of K_z in the stable, neutral and unstable boundary layer according to Eq. (C.36). The inversion height is 400 m. For comparison also some profiles of Yamada's second order closure model are given.
In the numerical transportmodel application an area averaged inversion height, $\overline{z}_i$, is used defined by:

$$\overline{z}_i(t) = \frac{1}{N'} \sum_{n=1}^{N'} z_i(n,t)\ , \qquad (C.37)$$

where $z_i(n,t)$ denotes the inversion height at the n-th gridpoint. The summation involves only gridpoints situated over land.

In Fig. 32 some typical profiles of the vertical eddy diffusivity are depicted for a stable, neutral and unstable situation respectively.

Appendix D: The analytical description of the fumigation process.

In Section 3.1.2. on fumigation, the dispersion of a continuous point source is described in an atmospheric boundary layer with a rising inversion and a uniform wind field. Initially the point source emits above the inversion layer, where turbulent diffusion is neglected. After some time the inversion passes the emission height, and the emitted plume -with infinitely small lateral dimensions- diffuses within the mixed-layer, where a uniform though time dependent diffusivity is assumed.
The concentration distribution within the rising mixed-layer originates, as it were, from two sources:
a. The entrainment of the plume (at time t_1), when the inversion passes the source can be represented by an instantaneous line source (ILS) with length equal to Ut_1, where U is the uniform wind velocity. The amount of instantaneous released material is equal to Qt_1, where Q is the real source strength(kgs^{-1}). The diffusing puff is uniformly advected by the mean wind, so that the solution for the ILS applies only in the region $U(t-t_1) \leq x \leq Ut$.
b. The continuous point source(CPS) starts to emit in the mixed layer at $t = t_1$. The solution for this source applies in the region $0 < x < U(t - t_1)$.

1. The diffusion equation

The equation of conservation of mass, which describes the dispersion is given by

$$\partial C/\partial t + U\, \partial C/\partial x = K(t)\, \partial^2 C/\partial z^2. \qquad (D.1)$$

For simplicity we treat the two-dimensional case, the extension to the 3-D one being trivial. Eq.(D.1) must be solved for both the CPS and the ILS. However, the ILS solution is uniform in x in the domain $U(t - t_1) \leq x \leq Ut$ and fits to the CPS solution in the region $0 \leq x \leq U(t - t_1)$, so that only the CPS solution is required. When the CPS solution is denoted by $C_{cps}(x,z,t)$, then the total solution is given by

$$C_t(x,z,t) = \begin{cases} C_{cps}(x,z,t) & 0 \leq x \leq U(t - t_1), \\ C_{cps}(U(t - t_1),z,t) & U(t - t_1) \leq x \leq Ut, \\ 0 & \text{else.} \end{cases} \qquad (D.2)$$

$C_t(x,z,t)$ denotes the solution in boundary-free space. When reflecting boundaries are present at $z = 0$ and $z = z_i(t)$, the solution should be replaced by

$$C(x,z,t) = \sum_{j=-\infty}^{j=+\infty} \{C_t(x,z-H-jz_i(t),t) + C_t(x,z+H-jz_i(t),t)\}, \qquad (D.3)$$

where H and z_i are the source- and inversionheight respectively.

2. The analytic solution

The solution of Eq.(D.1) with the boundary conditions

$$C \to 0 \text{ for } z \to \pm \infty, \; C(0,z,t) = Q/U \; \delta(z-H)$$
and $$C(x,z,0) = 0 \qquad (D.4)$$

can be obtained by the transformation

$$\tau = t - x/U \text{ and } s = x, \qquad (D.5)$$

yielding

$$U \; \partial C/\partial s = K(\tau+s/U) \; \partial^2 C/\partial z^2. \qquad (D.6)$$

Introducing $\partial q = K/U \; \partial s$, we obtain

$$\partial C/\partial q = \partial^2 C/\partial z^2, \qquad (D.7)$$

which can be easily solved. The result is

$$C_{cps}(q,z) = \frac{Q/U}{2(\pi(q-q_1))^{\frac{1}{2}}} \exp\{-\frac{(z-H)^2}{4(q-q_1)}\} \qquad (D.8)$$

Note that $q = \int_0^s K(\tau + s'/U)\, ds' = q(s,\tau)$, can be rewritten in the original variables by means of Eqs.(D.5).

Eqs. (D.3 and D.8) provide the final analytical solution. The approximation is made that the rate of inversion rise is slow compared with "diffusive velocity" so that the concentration distribution can adjust to the changing mixed-layer-height.

This condition can be expressed as:

$$\partial z_i/\partial t \ll \partial\sigma/\partial t\ , \qquad (D.9)$$

where $\sigma = (2K_z t)^{\frac{1}{2}}$.

The example given in table 3.II (section 3.1.2), was used for the analytical solution. The results are given in Fig. 33.

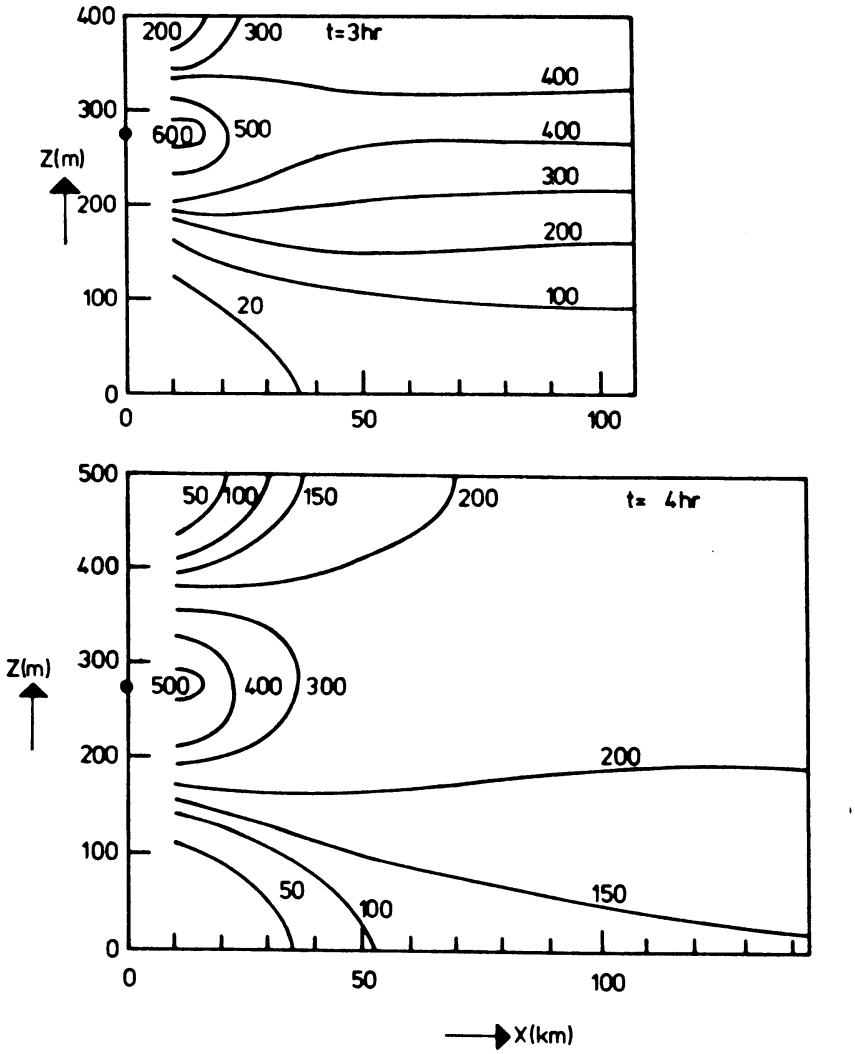

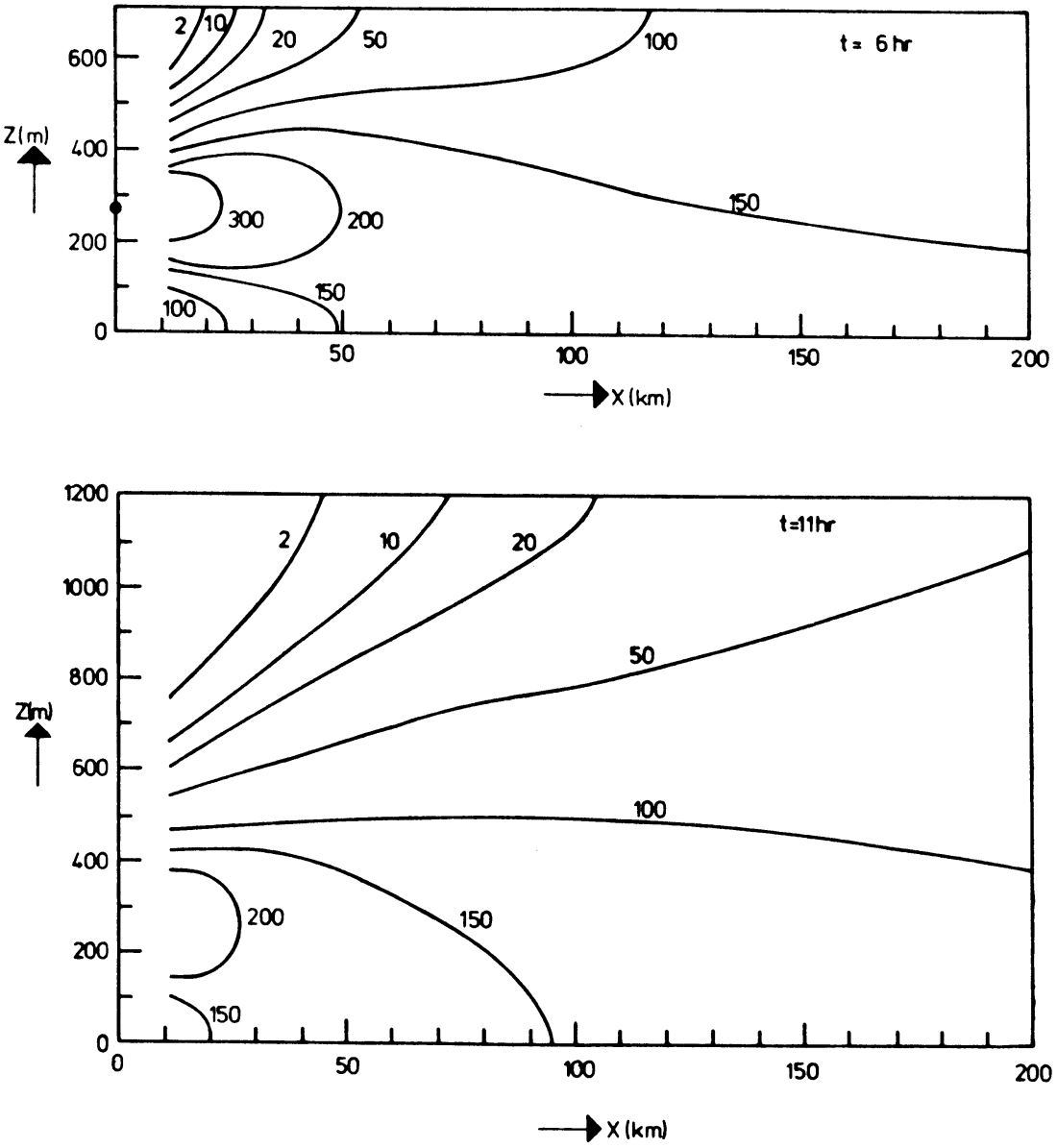

Fig. 33. Fumigation: Vertical cross section of the concentration [mgm^{-2}] obtained from the (approximate) analytical solution. For t = 3, 4, 6 and 11 hr after the start of release (cf. also fig. 7 and 8).

APPENDIX E: A short description of the computer programme

The KNMI air pollution transport model has been programmed in Fortran IV on a Burrough's 6800 computer. The model consists of a main programme and several subroutines. The specifications of the computation are read in two namelist statements. The meteorological and emission data are read from input files. The results of the computation are "hourly" written to an output file. We shall discuss the in and output files, the main program, the subroutines and the parameters in the common blocks below.

1. In and output files

In order to run the model the following input files were prepared.

namelist NL contains the specification of the run
NT contains the specification of the grid
file UXYZ/1 contains the u component of the velocity
file VXYZ/1 contains the v component of the velocity
file KVELD contains the eddy diffusivity values
file VD25XY contains the deposition velocity
file invhmean contains the mixing layer depth
file emissie contains the emission inventory
file adfusie/4 is the output file

The files UXYZ/1, VXYZ/1, KVELD and VD25XY are read unformatted. Each record contains 630 values. The first is the recordsize, i, the next i values are the actual elements to be read, the next is the number indicating time, followed by height of the field and two yet unused numbers.
The file invhmean is read unformatted. Each record contains the date and a value corresponding with the actual mixing layer depth.
The file emissie is read formatted. The first record contains nbron, the number of sources, and is read I5. The next nbron records are read (I4, 3F11.2, F11.4) resp. the source number, source position (m) 3x), and source strength.
The file adfusie/4 is written unformatted. The record length is 3468 words. The first record contains M1P1, NDMAX, IP, DTP, NPICT, LEVEL, which are

parameters for the KNMI plotting programme.
The next record contains the emission inventory on grid points. Following records contain the hourly concentration values.

The namelist NL contains the date MDTGØ, IHOEK (see below), IP the number of hours to be modelled, NDMAX the maximum number of layers that can be used, 13 variables for plotting purposes, RSTART must be set treu if the initial concentration is available, RREAD must be set true if the meteorological data must be read hourly, otherwise the data will be read once.
The namelist NT contains the discretization parameter, the time-step between input of data DTP (= 3600 s), IT1 the number of advection interations per DTP (IT1 should be even), LDIF (see below) and the gridpoint numbers M1 and M2 for the FFT routines.
IHOEK is a parameter which indicates the position of the model area within the (larger) area where the meteorological input data has been analysed. IHOEK = 0 places the model area in the SW-corner, and is to be choosen in cases with a SW wind, e.g. IHOEK = 8 x 25, 8 x 25 + 8 places the model area in the resp. SE, NW, NE corner of the analysis area.

LDIF indicates how many times per advection interation the diffusion interation has to be carried out. In cases with large vertical gradients LDIF should be larger than norma. LDIF = 2 is usually sufficient.

2. Main program and subroutines.

The main program organizes the run and calls the subroutines. The data is stored in common blocks. The gridpoint concentration values are stored in the blank common.
In order of their appearance in the program, the subroutines (and an indication of their function) are given below.

NORMAL / initiates the gridspecification for a normal computation. These default values may be overrules by the namelist statements. DX = DY = 20000, DZ = 50, M1 = M2 = 16, NDMAX = 12, DTP = 3600, IT1 = 6, LDIF = 2.

INFFT / computes the consts for the Fast Fourier Transformation package. It fills the common blocks CM, CF and CX.

SAFETY / checks the array dimensions and grid orientation.

PREMIS / reads the emission invetory. It fills the common block CE and the blank common with emission data.

INREAC / fills the common block CREAC with gridpoints reaction velocities. NB. At boundary points the velocities are larger in order to overcome boundary reflections.

INIT / fills the blank common with the initial concentration field. If RSTART is false it fills the blank common with zero's.

PREDIF / reads the files containing a. the mixing layer height, b. deposition velocity, c. eddy viscosity. It fills common block CN and decomposes the matrix concerning the vertical exchange of pollution. The results are stored in common block CK. If RREAD is false, PREDIF is called once. A check is performed on the actuality of the data.

WIND / reads the files containing the wind velocities and fills the common block CU. If RREAD is false, WIND is callled only once.

ADVEKT / controls the computation of the advection and reaction part of the transport by calling the subroutines RUNGE and REACTI.

RUNGE / computes the advection by time integration, the right hand side of the equation is computed by RLIDFF.

RLIDFF / computes the right hand side of the discretisized advection equation. Several subroutines from the FFT package are called.

REACTI / computes the reaction by time integration.

INFUUS / controls the calculation of the emissions. It archives the streamlines or inserts emissions by calling INEMIS.

INEMIS / computes the impact of a source.

DIFFUS / computes the diffusion by time integration.

MIXING / computes the mixing by time integration.

IDATG / computes the date.

IPUNT / computes the gridpoint number from the position (x,y,z).

3. Common blocks

The important variables of the common blocks and an indication of their usage

and the place where they are initiated is listed below.

CN /	DT /	timestep for diffusion	read from NT
	DZ /	vertical griddistance	read from NT
	M /	layer number	
	ND /	actual number of layers	/ computer in PREDIF
	NDMAX /	maximum number of layers	/ read from NL
	HMEAN /	mixing layer height = z_i	/ read in PREDIF
	DHMEAN /	difference between actual and former z_i	/ computed in PREDIF
	LMIX /	parameter describing whether the atmosphere mixes (LMIX = 1) of diffuses (LMIX = 0).	/ computed in PREDIF
CM /	Ml, etc /	constants concerning gridsize	/ read from NT and
	N /	number of gridpoints in a layer	/ computed in INFFT
	DX, DY /	grid distances	/ read from NT
	IHOEK /	orientation of model area in analysis area	/ read from NL
CF /	IFAXH /	arrays filled with data for use	/ computed in INFFT
	TRIGH /	in Fast Fourier Transforms	
CD /	DSR /	DSR contains the right hand side matrix	/ computed in PREDIF
	DSLLU /	DSLLU contains the upper and lower decomposition of the left hand side matrix of the diffusion equation.	
CU /	U, V /	velocities at gridpoints	/ read in wind
CX /	XMIN /	lower bounds of the grid	/ computed in INFFT
	YMIN /		/ from IHOEK
	ZMIN /		
CREAC/REAC	/	array containing the reaction velocites	/ computed in INREAC
CE /	NBRON /	number of sources	/ read in PREMIS
	CMIS /	emission data	/ read in PREMIS
	CARCH /	archive of streamlines	/ computed in INFUUS

The programme is on request available on tape.